

Article

Hydrochemical Indicator Analysis of Seawater Intrusion into Coastal Aquifers of Semiarid Areas

Jobst Wurl ^{1,*}, Miguel Angel Imaz-Lamadrid ², Lía Celina Mendez-Rodriguez ³
and Pablo Hernández-Morales ⁴

- ¹ Departamento Académico de Ciencias de la Tierra, Universidad Autónoma de Baja California Sur, Carretera al Sur km 5.5, La Paz 23080, Mexico
- ² Departamento Académico de Ingeniería en Pesquerías, Universidad Autónoma de Baja California Sur, Carretera al Sur km 5.5, La Paz 23080, Mexico
- ³ Centro de Investigaciones Biológicas del Noroeste S.C (CIBNOR), Calle IPN 195, La Paz 23096, Mexico
- ⁴ Departamento Académico de Ciencias Marinas y Costeras, Universidad Autónoma de Baja California Sur, Carretera al Sur km 5.5, La Paz 23080, Mexico
- * Correspondence: jwurl@uabcs.mx

Abstract: Saltwater intrusion into groundwater systems is a problem worldwide and is induced mainly by human activities, such as groundwater overexploitation and climate change. The coastal Los Planes aquifer in the southern part of the Baja California Peninsula (Mexico) is affected by seawater intrusion due to more than 40 years of groundwater overexploitation. A dataset of 55 samples was compiled, including 18 samples from our campaigns between 2014 and 2016. Several methods exist to define the impact of seawater in a coastal aquifer, such as the “seawater fraction”, the “Chloro-Alkaline Indices”, the “Hydrochemical Facies Evolution Diagram”, and the “Saltwater Mixing Index”. These methods provide reasonable results for most of the coastal zone of the Los Planes aquifer. A slight increase in mineralization was observed from 2014 to 2016 compared with the situation in 2003. However, in its northwestern part, samples from hydrothermal wells were not recognized by these methods. Here, the aquifer is affected mainly by thermal water with elevated mineralization, introduced through the El Sargento fault, a main fault, which cuts through the study area in the north–south direction. By considering known hydrothermal manifestations in the interpretation, samples could be classified as a combination of four end-members: fresh groundwater, seawater, and the composition of two types of thermal water. One thermal endmember with very low mineralization coincides with the thermal water described from the Los Cabos Block, where meteoric water represents the source (found in the Sierra la Laguna). The second endmember is comparable to coastal thermal manifestations where seawater represents the main source. Therefore, the higher mineralization in the northwestern zone is the result of the mobilization of thermal groundwater and direct mixing with seawater, which is introduced locally at the coast due to overextraction. This finding is important for future management strategies of the aquifer.

Keywords: hydrogeochemical characterization; seawater intrusion processes; geothermal water; mixing processes; cation exchange; Los Cabos block



Citation: Wurl, J.; Imaz-Lamadrid, M.A.; Mendez-Rodriguez, L.C.; Hernández-Morales, P. Hydrochemical Indicator Analysis of Seawater Intrusion into Coastal Aquifers of Semiarid Areas. *Resources* **2023**, *12*, 47. <https://doi.org/10.3390/resources12040047>

Academic Editor: Diego Copetti

Received: 24 January 2023

Revised: 26 March 2023

Accepted: 27 March 2023

Published: 7 April 2023



Copyright: © 2023 by the authors. Licensee MDPI, Basel, Switzerland. This article is an open access article distributed under the terms and conditions of the Creative Commons Attribution (CC BY) license (<https://creativecommons.org/licenses/by/4.0/>).

1. Introduction

Coastal aquifers are an important source of drinking water and water for agriculture and industry, especially in arid regions; however, these resources are significantly threatened by salinization due to seawater intrusion [1]. Seawater intrusion is one of the most severe environmental problems in coastal aquifers worldwide, exacerbated by the overexploitation of freshwater in coastal zones, and is susceptible to the influences of changing climates [2–4].

Mexico has experienced an important growth in population and agriculture surfaces in coastal areas over the last few years, which has led to the overexploitation of several aquifer systems [5]. In 2018, 105 aquifers were classified as overexploited, and 50 had salinization problems [6]. In 2020, the number of overexploited aquifers increased to 175 [7]. The problems of seawater intrusion are most notable in northwest Mexico [5] because of overexploitation and reduced annual precipitation, with an average of 200 mm in Baja California Sur (BCS) [6].

In the southern portion of the Baja California Peninsula, the salinization of aquifers has been related to agriculture, pollution, and seawater intrusion [8–12] without considering other phenomena such as hydrothermalism as a source of salinization. After 50 years of geothermal resource exploration in Mexico, it can be concluded that the peninsula has several regions with high potential [13]. Seven geothermal areas have been identified in the southern portion of the Baja California Peninsula. Two of these areas are related to recent volcanic activity, two are associated with the spreading tectonic zone in the middle of the Gulf of California, and the remaining three are due to movement through deep faults; the Los Planes aquifer (Figure 1) belongs to the last type [13]. In the Los Cabos region, four wells (SL1, SL2, SL4, SL5) were originally bored to obtain saltwater for a desalination plant project, but they resulted in the production of thermal water with an estimated deep reservoir temperature of 200 °C [13].

Our study area, the coastal Los Planes aquifer in the southern part of the Baja California Peninsula (Figure 1), is affected by seawater intrusion as a result of more than 40 years of groundwater overexploitation, as stated in former investigations (see Table 1) [14]. This is reasonable for most of the coastal zone, but it cannot be the explanation for the northwestern part of the aquifer because the water table and resulting flow lines indicate that this zone is still under an effluent flow regimen [14,15]. According to Del Rosal-Pardo, Busch et al., and Coyan et al. [16–18], at least four main faults with normal displacement and a north–south strike direction are affecting the Los Planes aquifer. These faults are related to hydrothermalism and may represent an additional source of salinity in the aquifer (Figure 1).

Table 1. Water balance in the aquifer between 2003 and 2020, after CONAGUA [7].

Year	Extraction Volume Million m ³ /Year	Recharge Million m ³ /Year	Deficit Million m ³ /Year
2003	12.29	9.89	−2.40
2007	12.29	8.40	−3.89
2013	12.29	8.26	−4.03
2015	12.29	8.40	−3.89
2020	13.10	8.40	−4.70

The purpose of this research is to assess the impact of seawater intrusion on the groundwater quality of a coastal aquifer in 2003 and in 2016 and to evaluate the extent to which hydrothermalism contributes to salinization. Different methods of analyzing groundwater affected by seawater intrusion and/or hydrothermal water are tested to determine how well they can distinguish between the two sources of salinization. Additionally, different types of hydrothermal water can be identified, and their corresponding mixing proportions with seawater can be calculated.

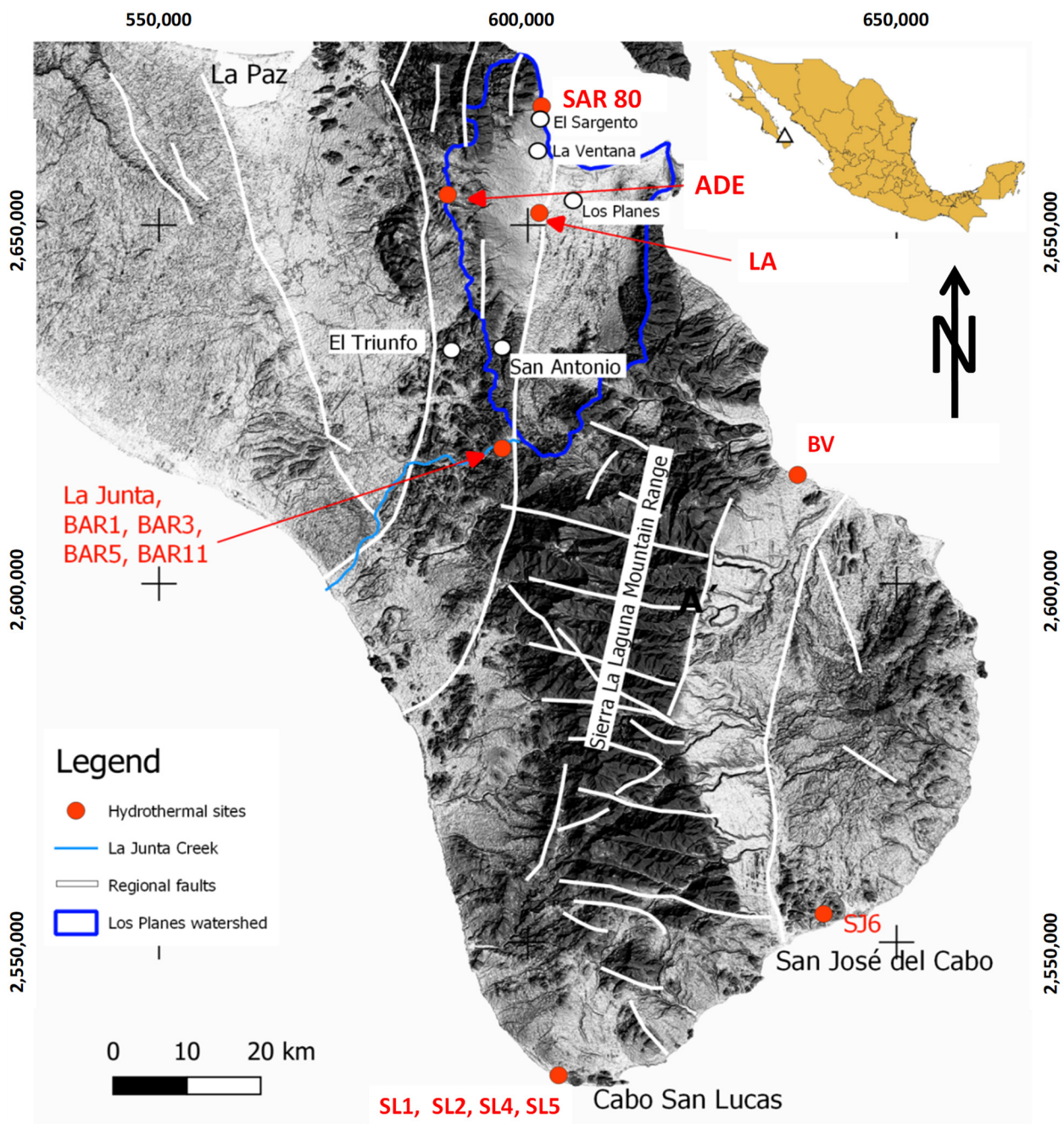


Figure 1. The southern tip of the Baja California Peninsula with main faults and important thermal manifestations, as described in the article. Surface relief was obtained from a 30 m DEM from NASA [19].

2. Regional Setting

The study was conducted in the southwestern portion of the State of BCS (Figure 1), within the Municipality of La Paz, in an area of 230 km² (Figure 2). The area is located at a distance of 50 km southeast of the city of La Paz. The Sierra de la Laguna is the main high mountain range in this region, with a maximum altitude of 2200 m. The mountains are formed by a massif crystalline basement, called the Los Cabos block [20], which is limited to the east by the San José del Cabo fault with a topographic escarpment above 1000 m [21,22]. The study area includes the San Juan de Los Planes basin (SJPB).

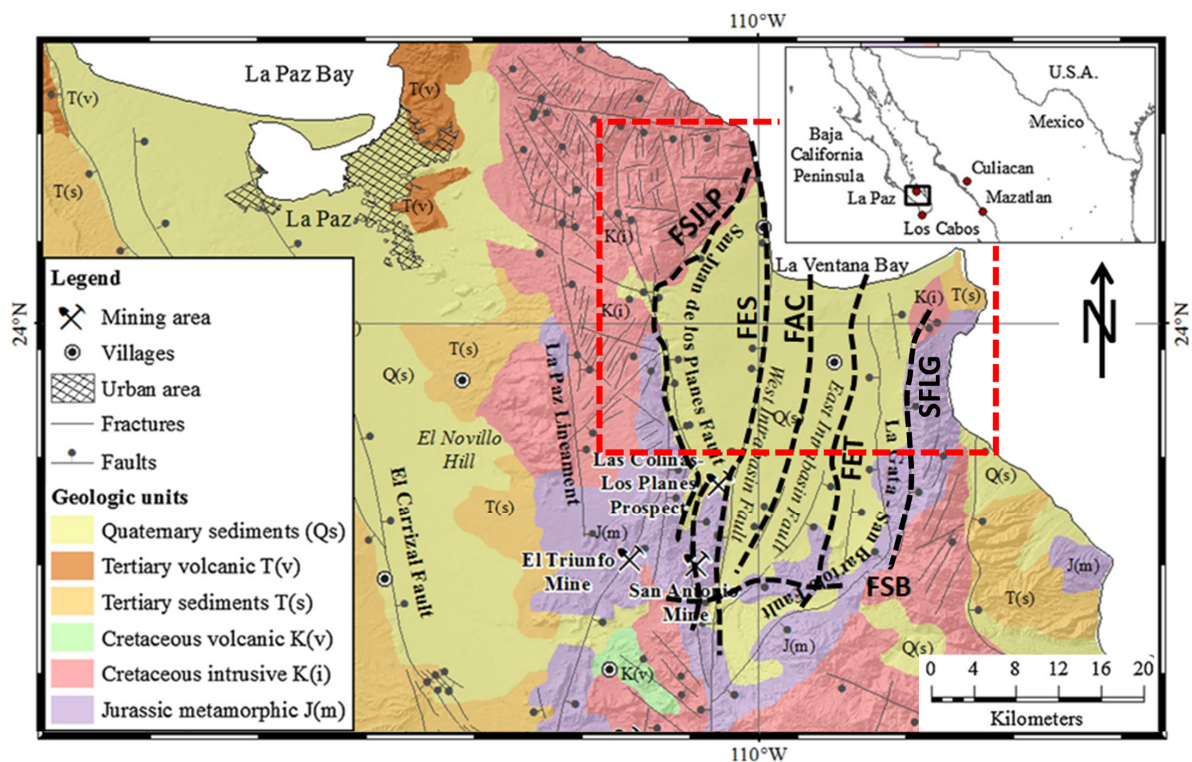


Figure 2. Geological map of the study area (dotted red line) with the main faults in the Los Planes basin: San Juan de Los Planes fault (FSJLP); El Sargento fault (FES); Agua Caliente fault (FAC); Tecuán fault (FET); La Gata fault (SFLG); and San Bartolo fault (FSB) [16–18].

2.1. Climate

CONAGUA [23] describes the climate as follows. According to the climate classification criteria proposed by Köppen, the prevailing climate in Los Planes is very dry (type BW) presenting most rain in summer and less in winter. The average annual temperature is between 22 °C and 24 °C. The highest monthly average temperatures occur in the summer, from June to September, varying from 27.3 °C to 29.8 °C; the absolute maximum temperatures recorded are from 41 °C to 45.5 °C. The coldest temperatures occur from December to February, with monthly mean values of 16.7 °C to 18.2 °C. The average annual rainfall for the basin is 281 mm and is affected by tropical cyclones during the rainy season (from May to November) [24,25]. The average rainfall varies from 175 mm/year in the coastal plain to 450 mm/year in the mountain range. The potential evaporation reaches up to 2000 mm/year. Tropical cyclones occur frequently during the rainy season (most likely between July and October).

2.2. Geological Setting

The Los Cabos Block, a batholithic massif of granitic and granodioritic rocks from the Cretaceous, appears as a mountainous complex that intrudes into Jurassic heterogeneous meta-sediments [22]. The block is partly covered by Miocene volcanic and volcanoclastic rocks from the Comondú Formation, which predates the opening of the Gulf of California [22]. The eastern part of the study area is formed by the Los Planes (SJLP) basin, a wide tectonic depression (pit) of elongated shape, with a preferential direction N-S that covers an area of 790 km². The basin represents an active graben structure, limited to the west by the San Juan de Los Planes normal fault (FSJLP) and to the east by the San Bartolo–La Gata normal fault (SFLG) (Figure 2). Additional north–south faulting is affecting the SJPB: El Sargento fault (FES); Agua Caliente fault (FAC); and Tecuán fault (FET) [16–18,26]. Busch et al. [17] verified the existence of the west-dipping intra-basin faults based on gravity sections and estimated that the FSJLP and FES reach depths of more than 3 km. Another fault, the

so-called San Bartolo fault (FSB), with a preferential E-W direction, is in the southern part of the Los Planes basin.

The San Juan de Los Planes (SJLP) basin is limited to the south by the Sierra de San Antonio, which is formed by granodiorites, granites, and metasedimentary rocks (tonalite, quartz diorite, quartz monzonite, gabbro, aplite andesite, and rhyolite dams). The Sierra La Gata forms the eastern limit of the Los Planes basin with a north–south orientation and is composed predominantly of intrusive rocks (granites, granodiorites, diorites, and tonalities) and metasedimentary rocks (originating from shale and sandstone and, to a lesser extent, graywacke and limestone) with a high degree of metamorphism [27]. The filling material is constituted by unconsolidated sediments of the Tertiary and Quaternary ages, consisting of fluvial sediments and alluvial deposits, mainly composed of medium- to coarse-grained sands, and dunes; the depth of the porous medium is variable within 30 to 250 m [28].

2.3. Hydrogeological Framework

The SJLP basin forms a semi-confined regional aquifer. It consists of unconsolidated granular sediments that cover an impermeable granitic basement [14]. The SJLP basin, which represents the lower part of the study area, is filled with sediments that consist of Quaternary alluvial deposits, mainly composed of medium- to coarse-grained sands (Figures 2 and 3). The hydraulic conductivity varies from 5 to 50 m/day. The aquifer is only occasionally recharged by the infiltration of rainwater and stream contributions [14]. The streams have an intermittent regime and infiltrate the alluvial plain; on occasion, the runoff reaches the Gulf of California.

The position of the aquifer basement and main structural elements are known mainly from geoelectrical resistivity and gravity sections [14,17]. Near the village of San Juan de Los Planes, a depth of more than 103 m is verified by four drillings; the base of the sandy aquifer consists of a 20 m layer of sandy silt [29] (Figure 3). CNA [14] reported an average hydraulic conductivity of 4.1 m/day, obtained from nineteen pumping tests (maximum value of 11 m/day and minimum value of 0.6 m/day); storage coefficients of 0.11 and 2×10^{-3} were obtained at two sites, indicating unconfined to semi-confined conditions.

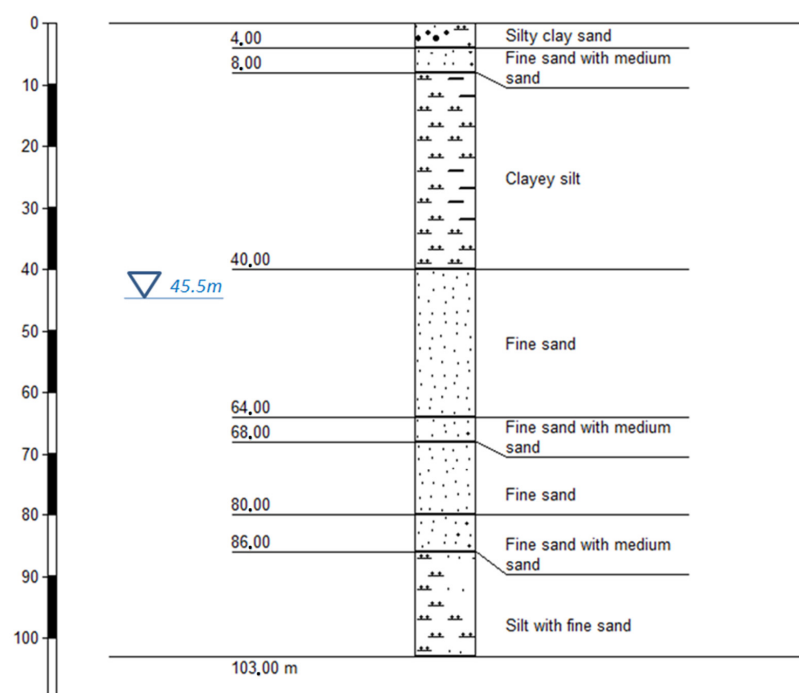


Figure 3. Typical sediments of the Los Planes aquifer in the center of the Los Planes aquifer (near Los Planes village; see Figure 4A), after TMI [29].

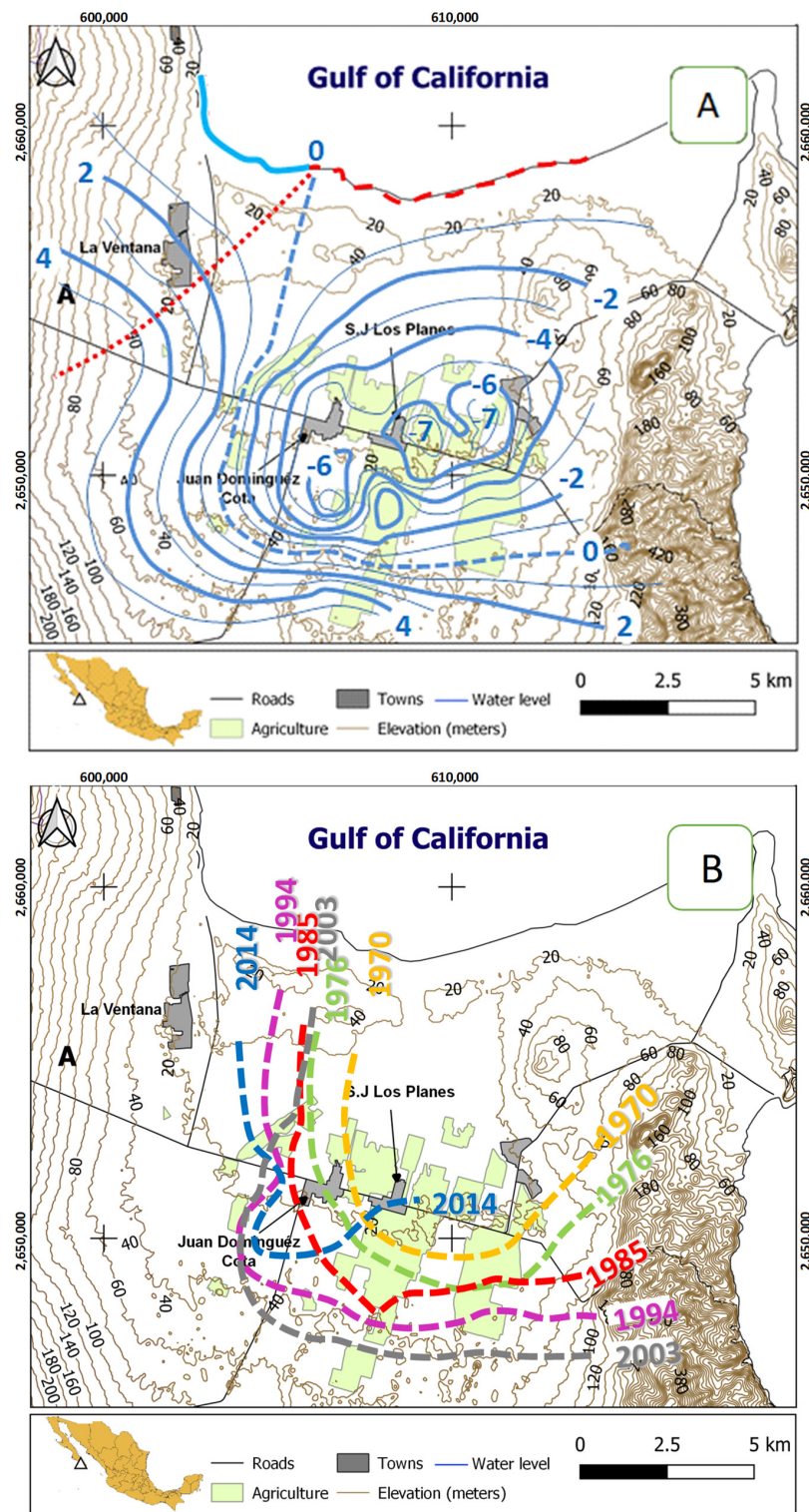


Figure 4. (A) The water table of the San Juan de Los Planes aquifer, after [14]. The dotted red line indicates the limit between the northeastern zone with groundwater flow toward the sea and the long dashed red line indicates the coastline with seawater intrusion (the red star indicates the position of a lithological column in Figure 3). (B) Variation of the 0 masl contour line of the water table between 1970 and 2014 [14,15].

The overexploitation of the aquifer started in the 1970s and caused the water table to lower by more than seven meters below sea level in the center of farmland near the village of San Juan de Los Planes (Figure 4; [14]). This changed the hydraulic gradient near the

coast, causing the intrusion of seawater at a length of 7 to 12 km inland [14] (Figure 4). All official balance calculations, elaborated by CONAGUA over the last 20 years, resulted in negative volumes per year due to overexploitation (Table 1).

Due to elevated groundwater extractions, a cone of depression formed (documented first in 1970), which deepened in the following years. In 2003, the lowest water levels were observed in the agricultural areas near the villages of Los Planes and Juan Cota Domínguez, reaching a minimum value of -7 m with respect to the sea level, consequently causing seawater intrusion. The 0 m contour line moved southward, with a maximum distance of 11 km, to the coastline in 2003 (Figure 4).

As is visible in Figure 4, an ongoing process of saltwater intrusion and water table lowering is notable from 1970 to 2003, followed by a phase of increasing water levels between 2003 and 2014; meanwhile, the northwestern part (near La Ventana) presented decreasing water levels between from 1970 to 2014.

2.4. Geothermal Framework

The hydrothermal activity on the peninsula is linked to regional normal striking faults that allow for the deep penetration of water in areas of high heat flow; these faults are related to the extensional tectonics of the Gulf of California in the Tertiary [13,30,31]. Since the installation of the geothermal power plant Tres Virgenes in the northern part of the peninsula in 1997, many new sites with geothermal manifestations on the peninsula of Baja California have been discovered. A compilation of the main sites was presented by Arango-Galván et al. [13], who defined 14 geothermal areas and described their characteristics.

In the western part of the Los Planes basin, several geothermal wells and springs are situated along the coastline in a north–south direction. These thermal manifestations follow the north–south striking El Sargento fault (FES). About one kilometer north of the village of El Sargento, a geothermal anomaly is situated at the beach called “Agua Caliente”. A water temperature of 82 °C was recorded in April 2016 at this beach at a 70 cm depth (Figure 5). Four wells are situated along the El Sargento fault (FES), and one is close to the Los Planes fault (Figure 5).

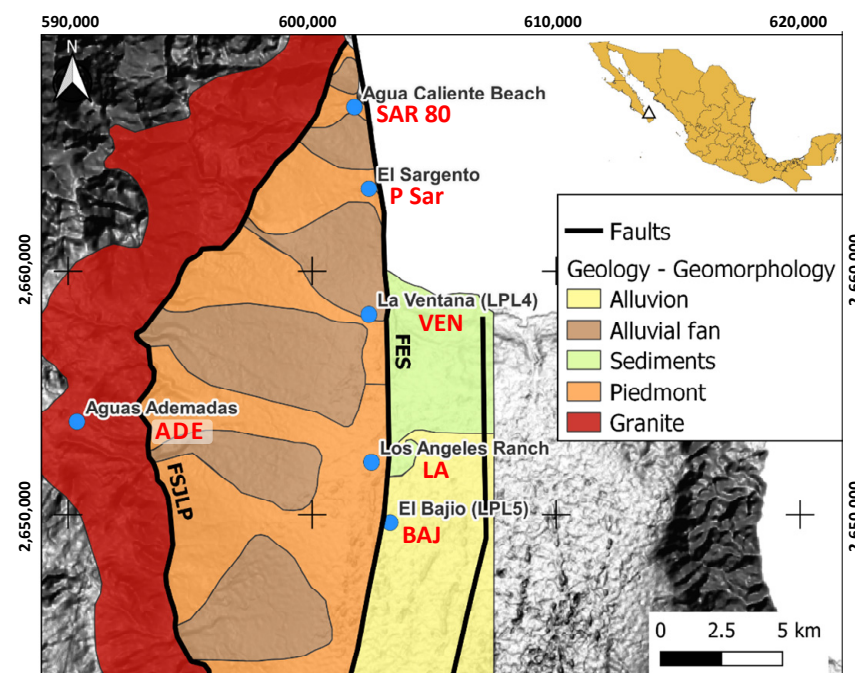


Figure 5. Geologic map of the northwestern part of the Los Planes aquifer with the main faults (El Sargento fault (FES) and San Juan de Los Planes fault (FSJPL)) and related geothermal manifestations (blue points).

2.5. Agriculture and Industrial Activities

Agriculture represents the main economic activity in the Los Planes watershed, with a total irrigated surface of 820 ha [14]. Chile represents the most important crop, taking up 61% of the irrigated surface [14]. Only 16.5 percent of the irrigated surface is used during the summer season, mostly for corn production. The total water volume for irrigation is 6.5 million m³, with a resulting irrigation return flow of 16.6% (Table 2).

Table 2. List of the main crop types; corresponding irrigation systems, irrigated surfaces, and water volumes; and the resulting return flows [14].

Season	Crop	Irrigation System	Irrigated Surface (ha)	Net Volume Used (m ³)	Irrigation Return (m ³ /Year)
Winter	Chile	Drip	160	1,200,000	48,000
	Chile	Flood gates	340	2,550,000	484,500
	Tomato	Drip	60	462,000	18,480
	Corn	Irrigation channel	65	286,000	111,540
	Cotton	Flood gates	30	210,000	39,900
	Cucumber	Drip	50	200,000	8000
	Beans	Aspersión irrigation	50	190,000	26,600
	Subtotal		755	5,098,000	737,020
Summer	Corn	Irrigation channel	135	594,000	231,660
	Subtotal		135	594,000	231,660
Perennial	Alfalfa	Aspersión irrigation	50	600,000	84,000
	Fruit trees	Aspersión irrigation	15	180,000	25,200
	Subtotal		65	780,000	109,200
Total			955	6,472,000	1,077,880

At present, there is no industrial activity of importance going on, but the western part of the Los Planes aquifer is affected by historical gold mining. This activity took place in the region between 1878 and 1911, including the area around the village of San Antonio. Carrillo [32] described three types of ore deposits in the San Antonio–El Triunfo mining district, where epithermal veins represent the main type, containing high sulfide concentrations associated with gold and silver (gold associated with arsenopyrite). The ore processing techniques employed included cyanide-based milling, gold ore roasting, and amalgamation, among others [33]. An estimated 800,000 to 1,000,000 tons of mine waste materials were scattered in an area of approximately 350–400 km², which contained different byproducts resulting from arsenopyrite oxidation, mainly arsenolite (As₂O₃) [34]. Therefore, the region shows contamination problems with high concentrations of As, Cd, Pb, and Zn in the mine waste [35,36]. The contamination was widely distributed, mainly by winds and runoff from tropical storms, so the contamination was distributed in arroyo sediments at distances of up to 18 km.

3. Materials and Methods

3.1. Water Samples Documented in Former Studies (for Water Quality and Seawater Intrusion Estimation)

A compilation of own and published data was elaborated to describe the seawater intrusion status in 2003 and from 2014 to 2016 (documented in the Supplementary Materials File).

The CNA (2003) [14] water sampling campaign included 45 sampling sites, 19 of which were coastal wells, included in this study. The in situ measurements included pH, temperature, dissolved oxygen, electrical conductivity, and alkalinity. The water samples were collected in HDPE bottles and filtered, preserved, and sent to specialized labs for the determination of major ions and cations, as well as metals [14].

The dataset for 2014–2016 included seven wells (9, 10, 14, 16–19) located in the central part of the Los Planes basin and documented by Briseño-Arellano [15]. Another 16 samples from coastal wells were taken in 2016, including 12 sites where data from 2003 were available and 4 at known hydrothermal anomalies (3 wells and one spring (Agua Caliente); see Figure 6). In all samples, the field measurements included pH, temperature, dissolved oxygen, and electrical conductivity. All samples were filtered through 0.45 μm membrane filters in the field and collected in polyethylene bottles, previously washed, and samples were stored in ice boxes at $<4\text{ }^{\circ}\text{C}$ to minimize bacterial activity. The samples collected for cation analysis were acidified with concentrated Suprapur HCl or concentrated Suprapur HNO₃ to obtain pH < 2 . The samples were analyzed in specialized laboratories using ICP-OES (metals) and ion chromatography (major ions) following QA/QC protocols for the analysis of water [37,38]. Blanks were included during sampling trips [39]. Values for pH, electrical conductivity, carbonates, chlorides, and sulfates were determined in the field [37,40,41].

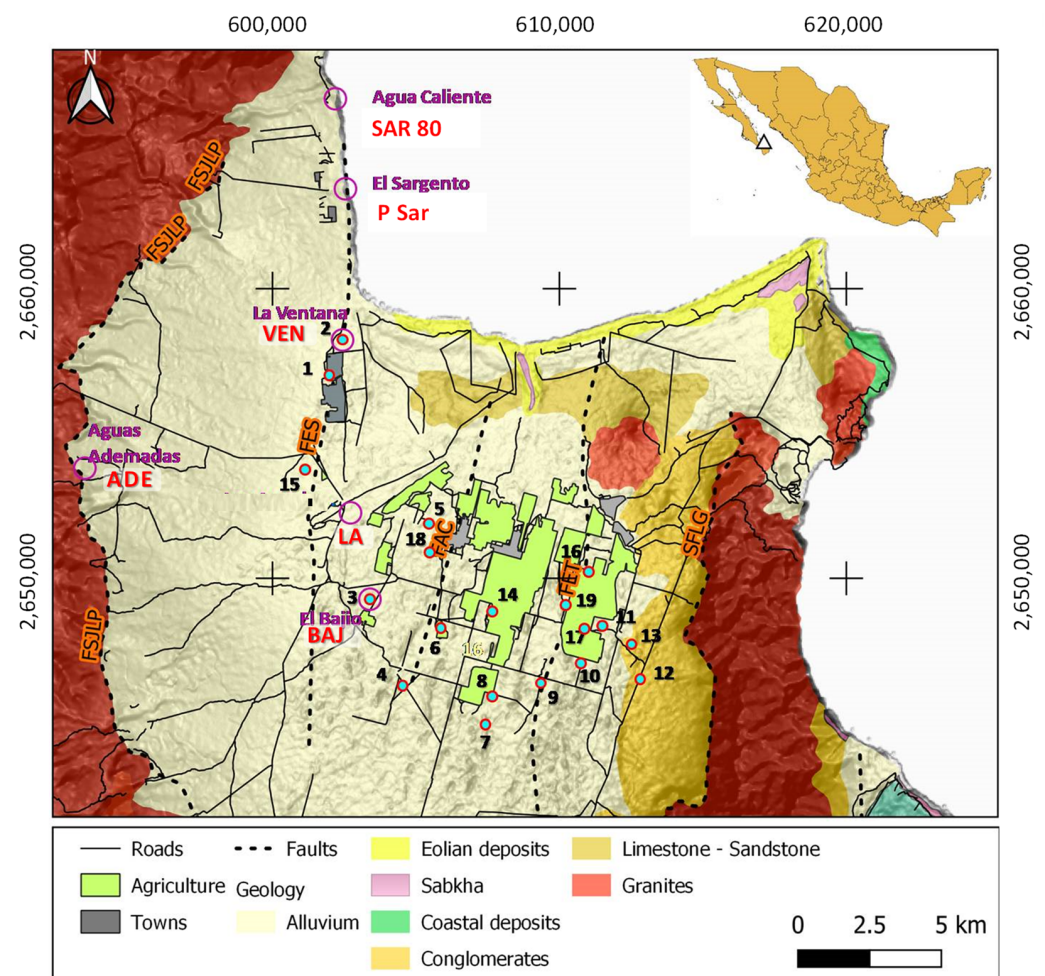


Figure 6. Position of 19 wells with hydrochemical data from 2003 and 2014 to 2016 (green dots) and wells with elevated temperatures (red dots).

3.2. Recognizing Seawater Intrusion by Different Methods

Seawater intrusion is a dynamic process that results from periodic changes in the recharge–discharge balance of the aquifer, where any direct or indirect influence on the aquifer’s water balance affects the position and movement of the seawater interface [42,43]. The variations in groundwater chemistry then result from differences in recharge-source chemistries, varied aquifer materials, and fluctuations in groundwater flow [44]. To recognize the effects of seawater intrusion on the hydrochemical composition of groundwater,

several parameters can be considered, such as the higher total mineralization or the chloride concentration of the groundwater [45]. Electrical conductivity (EC) is another basic indicator used to determine whether an aquifer is contaminated and also indicates if this process is increasing [45]. Commonly, an EC of less than 1000 $\mu\text{S}/\text{cm}$ indicates that the groundwater is under normal conditions [46]. There are several indicators and graphical representation methods to understand the hydrochemical characteristics and facies of freshwater–saltwater systems. However, groundwater may also acquire salinity through contamination from agriculture, industries, improper sewage disposal, domestic wastewater, the mobilization of deeper groundwater or thermal water, etc. The following methods were applied to recognize the seawater fraction in the groundwater, ion exchange processes, and evaporation processes and obtain information on anthropogenic contamination and geothermal influence. A flowchart (Figure 7) explains the sequence in which these methods were applied.

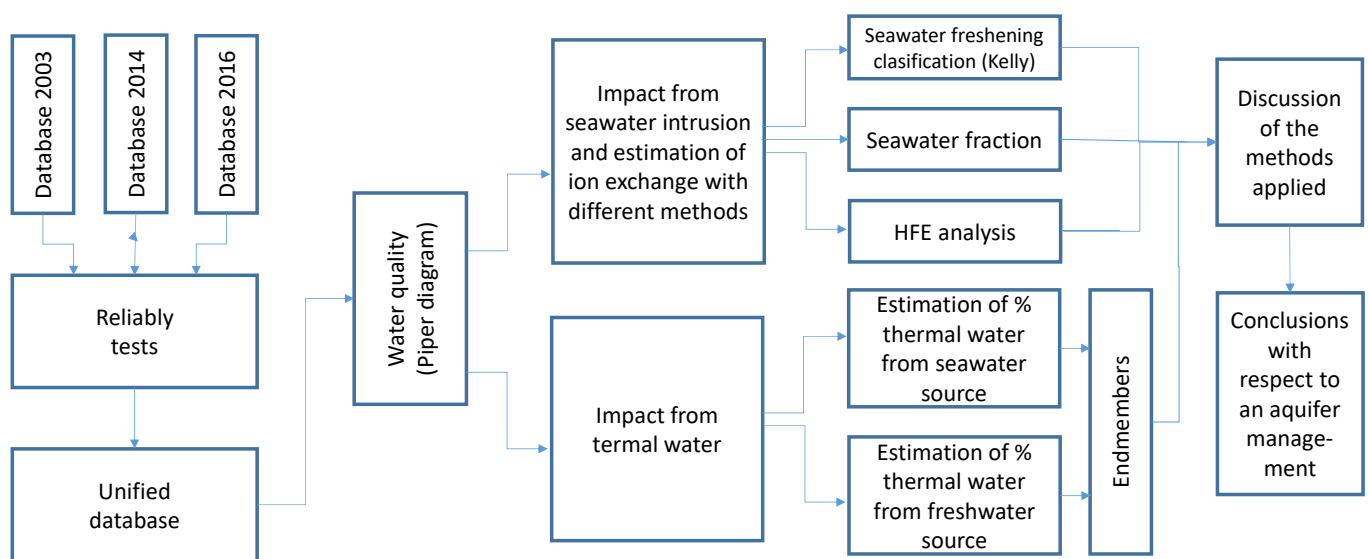
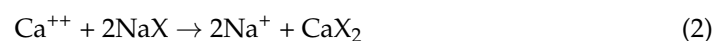


Figure 7. The flowchart of the hydrochemical data interpretation.

3.2.1. Classification of Seawater Freshening

Kelly [47] defined seven different criteria ranging from fresh groundwater to seawater to interpret the effects of saline water intrusion in a Piper diagram. A “mixture” field between the seawater and freshwater field indicates conservative mixing without ion exchange. As the water is mixed in the presence of aquifer materials, ion exchange may occur, modifying the chemical composition of the groundwater. This will cause the sample position in the diagram to migrate from the conservative mixing line to the upper part of the diamond field during the intrusion phase (after Equation (1)) and downward during the refreshment phase (Equation (2)):



3.2.2. Calculation of the Seawater Fraction and Mixing Index Seawater Fraction

The mixing reactions that occur in the transition zone between fresh groundwater and seawater can be recognized by comparing the measured water composition with the one calculated for the conservative mixing of freshwater and seawater [48]. The freshwater–seawater mixing proportion in each sample was calculated using the Appelo and Postma

formula [41] and assuming that there were no other contributions to salinity other than freshwater and seawater:

$$\text{Seawater fraction : } f_{\text{sea}} = \frac{m_{\text{sample}} - m_{\text{fresh}}}{m_{\text{sea}} - m_{\text{fresh}}} \quad (3)$$

where m is the molar concentration of the anion (Cl^- or Br^-) in the sample in freshwater (fresh) or seawater (sea).

Saltwater Mixing Index (SMI)

In open seawater, the conservative elements are found in constant proportions to one another and to salinity, although salinity varies. All the major ions in seawater, except for bicarbonate, and some trace elements are included in this group [49]. Therefore, element ratios can be used as an indicator of seawater intrusion. The "Saltwater Mixing Index" (SMI) proposed by Park and Aral [50] can be used to estimate the relative degree of saltwater/brackish water mixing with freshwater, taking four major ions into account; it is calculated as follows:

$$\text{SMI} = a * \frac{C \text{Na}^+}{T \text{Na}^+} + b * \frac{C \text{Mg}^{2+}}{T \text{Mg}^{2+}} + c * \frac{C \text{Cl}^-}{T \text{Cl}^-} + d * \frac{C \text{SO}_4^{2-}}{T \text{SO}_4^{2-}} \quad (4)$$

where letters a , b , c , and d represent the relative concentration proportion of ions Na^+ , Mg^{2+} , Cl^- , and SO_4^{2-} in seawater ($a = 0.31$, $b = 0.04$, $c = 0.57$, $d = 0.08$); C is the measured concentration (in mg/L) of the ions in the groundwater [51]. The letter T represents the estimated regional threshold values, which were obtained, for example, from probability curves [51,52]. A probability plot was elaborated to calculate the threshold values for the natural concentrations of the major ions in the fresh groundwater of the study area. Based on a probability plot of a certain ion, the group of samples with to the lowest concentration was separated, and the mean value and standard deviation were obtained. Finally, the threshold values were calculated from the mean concentrations plus 2 standard deviations. The following threshold values were obtained: Na^+ (85.4 mg/L), Mg^{2+} (9.5 mg/L), Cl^- (60.5 mg/L), SO_4^{2-} (35 mg/L), HCO_3^- (160.7 mg/L), Ca^{2+} (22.3 mg/L), K^+ (1.6 mg/L).

3.2.3. Hydrochemical Facies Evolution Diagram

The hydrochemical facies evolution diagram (HFE-D), proposed by Giménez-Forcada [42], allows for the identification of the origin of groundwater salinization; it also indicates different freshening or salinization trends in a coastal aquifer [53,54]. In the HFE-diagram, the abscissas represent the evolution of % $\text{Na}^+ + \text{K}^+$ and % Ca^{2+} (or % Mg^{2+}), and the ordinates identify the evolution of % Cl^- and % $\text{HCO}_3^- + \text{CO}_3^{2-}$ (or % SO_4^{2-}). The percentages are estimated based on total cation and anion concentrations, including those not explicitly delineated (usually Mg^{2+} or SO_4^{2-}); based on a percentage of ions of more than 50%, the following four main facies can be distinguished: Na- HCO_3 (salinized water where direct cation exchange reactions occurred), Na-Cl (seawater), Ca- HCO_3 (freshwater), and CaCl₂ (salinized water where reverse cation exchange reactions took place). If a percentage of an ion is less than 50%, then the prefix "Mix" is added in case the corresponding freshwater corresponds to the CaHCO₃ type [42,53].

3.3. Thermal Water

Scatter diagrams and a diagram after Giggenbach and Goguel [55] were used to recognize two hydrothermal water endmembers on the Baja California Peninsula and their mixing relationships with seawater. The diagram is based on the relationship between $\text{Mg}/(\text{Mg} + \text{Ca})$ and $\text{K}/(\text{K} + \text{Na})$. A curved line indicates the existence of water-rock equilibrium at different temperatures.

The sampling sites influenced by geothermal activity are shown in Figure 5. Four wells and one spring are situated close to the El Sargento fault, and another well is located close to the Los Planes fault. At these sites, a mixture of groundwater and geothermal water can be expected. Analyses from another 11 known hydrothermal sites of the region were also included in the interpretation: 4 from thermal manifestations in the Sierra La Laguna mountains [39], 5 described by López-Sánchez et al. [56] (4 wells are located near Cabo San Lucas and 1 is located near San Jose del Cabo), and 1 well at Buenavista reported by Hernández-Morales and Wurl [57].

4. Results and Discussion

4.1. Water Quality

Groundwater presented a wide range of total dissolved solids (TDS) for the whole dataset from freshwater to brackish water. In 2003, the TDS ranged from 309 to 2007 mg/L with a median value of 907 mg/L. For 2014–2016, salinity ranged from 340 mg/L to 4145 mg/L, with a median value of 1190 mg/L. The pH ranged from 6.9 to 8.2 in 2003 and 7.2 to 8.5 for 2014–2016 (Table 3). Changes in water quality were notable with an increase in the total mineralization (TDS +31.2%) and in Na^+ (+33.7%), Mg^{2+} (46.1%), Cl^- (44.6%), SO_4^{2-} (20.7%), and HCO_3^- (23.0%) as ions. A slight reduction was observed for Ca^{2+} (−1.5%).

Table 3. The results of the physicochemical parameters from the 2003 and 2014–2016 campaigns.

Campaign		Temp	pH	Ca^{2+}	Mg^{2+}	Na^+	K^+	HCO_3^-	SO_4^{2-}	Cl^-	TDS
		°C		mg/L	mg/L	mg/L	mg/L	mg/L	mg/L	mg/L	mg/L
2003 *	Minimum	38.6	6.9	13.30	4.90	66.00	2.30	91.12	23.00	50.30	309
2003 *	Maximum	32.0	8.2	172.40	78.80	550.00	19.60	257.28	375.00	893.40	2007
2003 *	Average.	30.0		77.81	31.90	205.52	6.22	152.02	137.47	309.66	907
2003 *	St. Dev.	1.8		48.84	24.68	145.79	4.31	43.86	105.85	264.69	580
2014–2016 **	Minimum	30.5	7.2	9.37	8.38	63.01	0.86	122.00	21.78	45.65	340
2014–2016 **	Maximum	37.8	8.5	213.62	176.93	1239.5	43.25	316.07	454.61	1917.4	4145
2014–2016 **	Average.	26.9		76.66	46.62	274.74	7.02	186.94	158.14	447.71	1190
2014–2016 **	St. Dev.	2.35		57.51	43.65	269.87	9.52	47.68	150.93	456.44	916

* Taken from [14]; ** data is from this study and from [15]. St. Dev. = standard deviation.

Regarding water quality for human use, 31.6% and 47.4% of the samples from 2003 did not comply with the Mexican drinking water standard (NOM-127-SSA1-1994) for Na^+ and Cl^- , respectively. For 2014–2016, 36.8%, 47.4%, and 10.5% of the samples did not comply with the standard for Na^+ , Cl^- , and SO_4^- , respectively.

4.2. Groundwater Types

The relationship between major ions can be observed in the Piper diagram for 2003 and 2014–2016 (Figure 8A,B). In both diagrams, sodium is the most dominant cation, while chloride and bicarbonates are the most abundant anions. Interpreting the Piper diagram after the Kelly classification [47], it can be observed that in 2003 and 2014–2016. A total of 13 samples corresponded to the “intrusion” or “conservative mixing” fields. A general trend of increasing salinization between 2003 and 2014 to 2016 was observed; however, in some wells, freshening occurred. In 2003, three samples fell in the “freshening” and “slight freshening” fields, while for 2014–2016, there were four samples in these fields (Table 4).

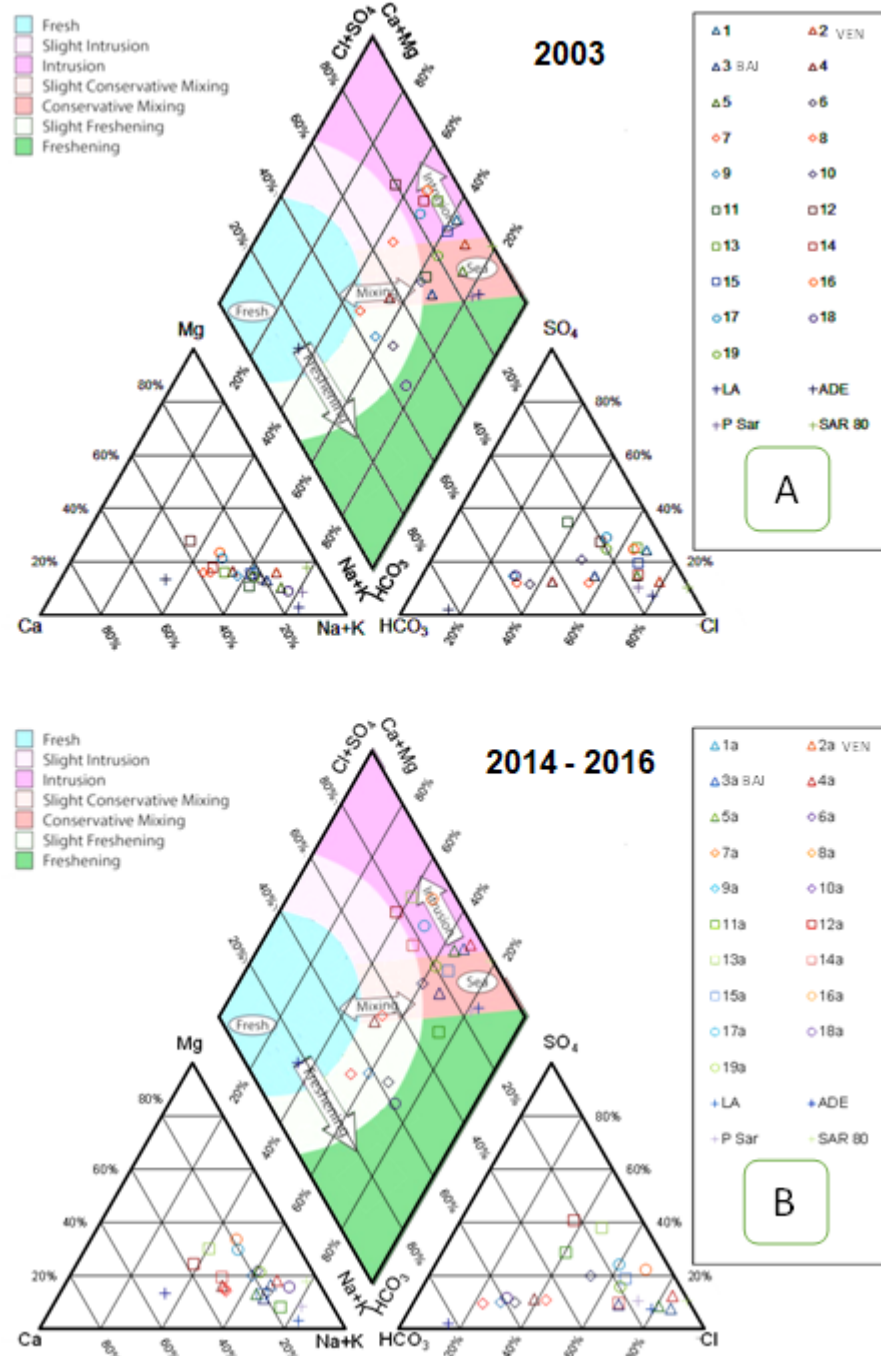


Figure 8. Piper diagram with seawater-freshening classification, after Kelly [47]: (A) 2003; (B) 2014–2016.

Table 4. Classification of 19 water samples, after Kelly [47].

Classification	2003	2014–2016
Intrusion	7	8
Conservative mixing	6	5
Slight conservative mixing	3	2
Slight freshening	2	2
Freshening	1	2
SUMA	19	19

4.3. Calculation of the Seawater Fraction Based on Ion Ratios

In open seawater, the conservative elements are found in constant proportions to one another and to salinity, although salinity varies. All the major ions in seawater, except for bicarbonate, and some trace elements are included in this group [49]. Therefore, element ratios can be used as an indicator of seawater intrusion. The calculated seawater fractions (%) are provided in Table 5).

Table 5. Calculated seawater fractions (%) for 2003 and 2014–2016 and their differences (%).

Ref.	<i>f_{sea}</i> %	<i>f_{sea}</i> %	<i>f_{sea}</i> %
	2003	2014–2016	Difference
1	3.69	4.11	0.42
2 VEN	4.21	9.39	5.18
3 BAJ	0.49	0.97	0.48
4	0.09	0.09	−0.00
5	1.11	3.04	1.93
6	−0.03	−0.03	−0.00
7	0.01	−0.08	−0.09
8	0.47	0.24	−0.23
9	−0.03	−0.01	0.02
10	0.43	0.67	0.23
11	0.29	0.26	−0.03
12	1.67	1.23	−0.44
13	1.76	1.61	−0.15
14	1.05	0.80	−0.24
15	3.64	2.63	−1.01
16	1.73	4.17	2.44
17	1.27	1.87	0.60
18	−0.05	−0.02	0.03
19	0.49	0.87	0.38
LA *		3.1	
SAR *		88.5	
P Sar *		3.6	
ADE *		−0.2	

* At this site there was no data available from 2003.

Although an average increase of 0.5% in the seawater fraction was obtained for all samples from 2014 to 2016 compared with the situation in 2003, most wells showed a low seawater fraction (below 1% in 53% of the samples from 2003 and 58% from 2014 to 2016). According to Mahlkecht et al. [5], and regarding human uses, mixing only 2% seawater into a freshwater aquifer exceeds organoleptic objectives for the upper limit of chlorides, while mixing in 4% will make water mostly unusable, and 6% will make it only suitable for cooling and flushing purposes. In 2003, three samples surpassed the 2% limit, and in 2014–2016, five samples did so (Table 6). In 2003, one sample also surpassed the 4% limit, and three surpassed the limit for 2014–2016, of which one sample even surpassed the 6% limit.

Changes in the calculated seawater fraction (of less than $\pm 0.1\%$) were observed at six wells; eight showed an increase (red color) of up to 5.2%, and five showed a decrease with a maximum of 1%. However, the salinity of freshwater can vary depending on other factors such as the infiltration of irrigation return flows. Stigter et al. [58] defined an increase in salinity from a factor of three in a rural aquifer in Portugal with heavy pumping rates, and [5] used a factor of five for the more urban-influenced La Paz aquifer in northwestern Mexico. Under both definitions, only well 2 showed a clear increase in salinity.

4.4. Salinity Origin after the Hydrochemical Facies Evolution Diagram

In shallow sedimentary aquifers, groundwater evaporation, cation exchange, ion effects, and salt effects are important geochemical factors that occur widely. Cation exchange

involves the replacement of the bivalent cations Ca^{++} and Mg^{++} in the aquifer matrix with the monovalent cations Na^+ and K^+ in groundwater see Equations (1) and (2).

The hydrochemical facies evolution diagram (HFE-D) was applied to the samples for 2003 and 2014–2016 to understand the state of the Los Planes aquifer and discriminate between the two principal phases (intrusion or freshening). Both phases are separated in the HFE-D by the conservative mixing line (blue line in Figure 9).

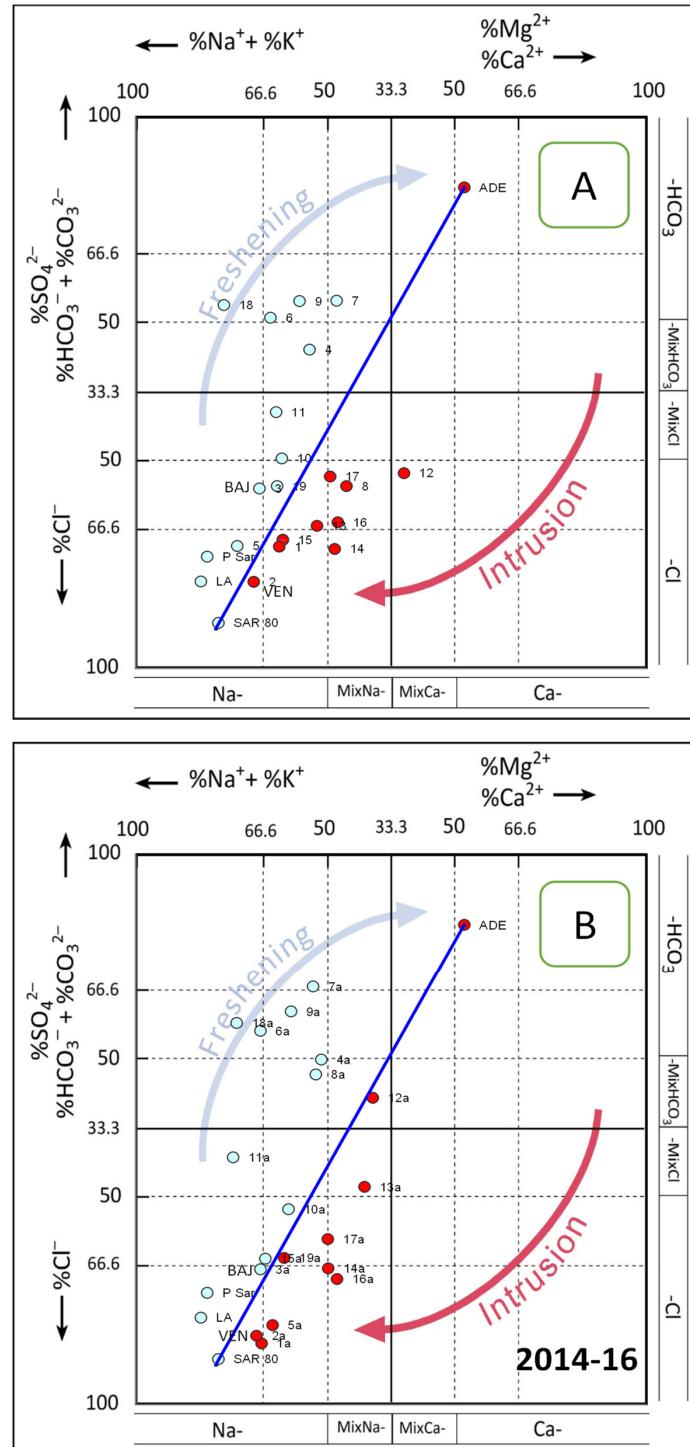


Figure 9. HFE-diagram for 2003 (A) and 2014–2016 (B).

In 2003, 10 samples can be identified as the freshening phase and 9 as the salinization phase. For 2014–2016, only 9 samples can still be defined as the freshening phase, but 14 can

be identified as the salinization phase, an indication that seawater intrusion was advancing (Figures 9 and 10). The diagram allows us to identify five substages for each phase: f1, f2, f3, and f4 for freshening and FW for freshwater; i1, i2, i3, and i4 for the salinization and SW for saltwater (Figure 9). Four samples (LPL 5, 6, 7, and 16) show a shift from freshwater toward seawater intrusion (Table 6).

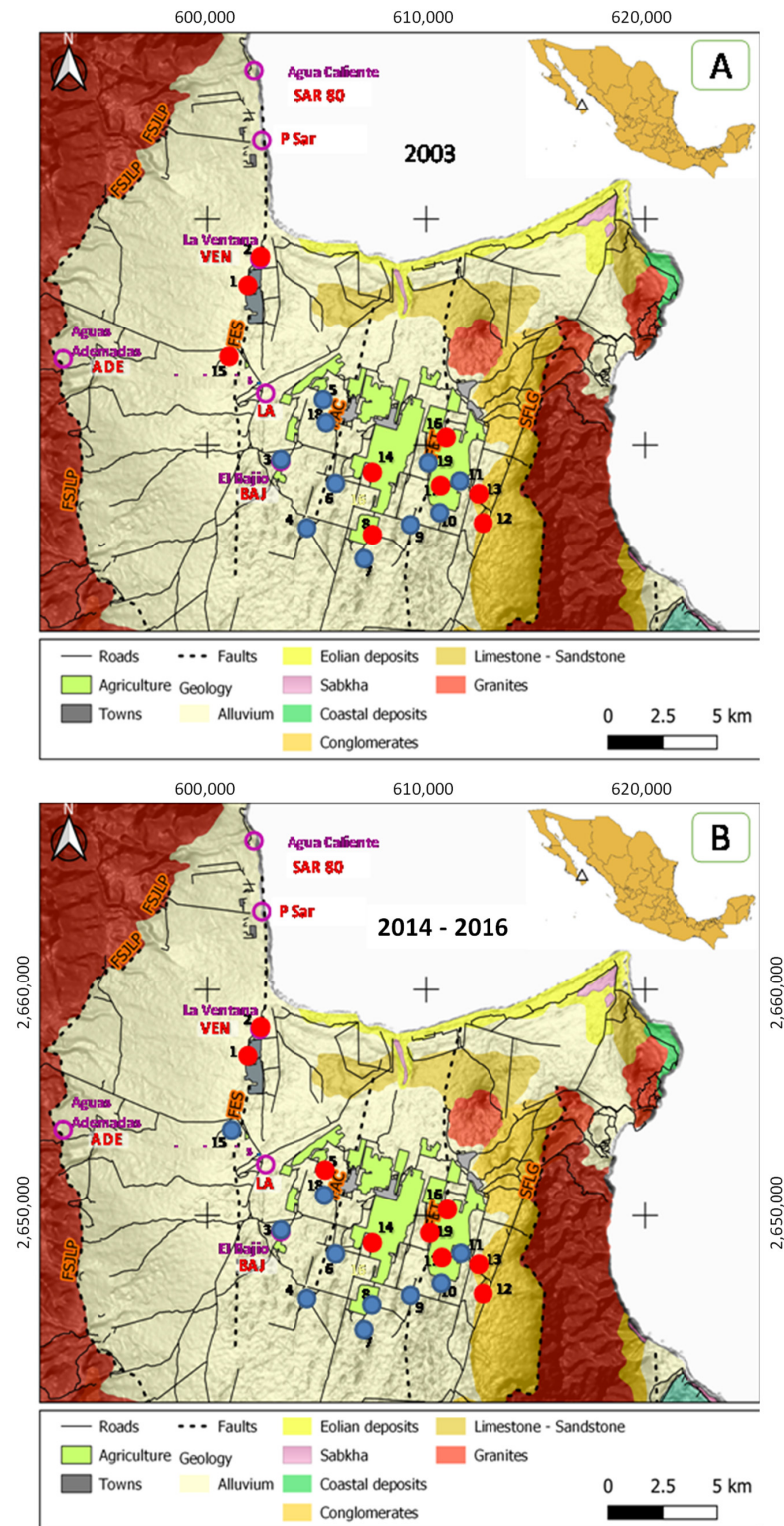


Figure 10. Changes in seawater intrusion between (A) 2003 and (B) 2014–2016, as defined by the HFE diagram.

Table 6. Facies evolution between 2003 and 2014–2016.

Site		2003		2014–2016		
No.	Phase	Facies		Phase	Facies	
1	Intrus.	Na	Cl	Intrus.	Na	Cl
2 VEN	Intrus.	Na	Cl	Intrus.	Na	Cl
3 BAJ	Fresh.	Na	Cl	Fresh.	Na	Cl
4	Fresh.	Na	MixHCO ₃	Fresh.	Na	HCO ₃
5	Fresh.	Na	Cl	Intrus.	Na	Cl
6	Fresh.	Na	HCO ₃	Fresh.	Na	HCO ₃
7	Fresh.	MixNa	HCO ₃	Fresh.	Na	HCO ₃
8	Intrus.	MixNa	Cl	Fresh.	Na	MixHCO ₃
9	Fresh.	Na	HCO ₃	Fresh.	Na	HCO ₃
10	Fresh.	Na	MixCl	Fresh.	Na	Cl
11	Fresh.	Na	MixCl	Fresh.	Na	MixCl
12	Intrus.	MixCa	Cl	Intrus.	MixNa	MixSO ₄
13	Intrus.	Na	Cl	Intrus.	MixNa	MixCl
14	Intrus.	MixNa	Cl	Intrus.	MixNa	Cl
15	Intrus.	Na	Cl	Fresh.	Na	Cl
16	Intrus.	MixNa	Cl	Intrus.	MixNa	Cl
17	Intrus.	MixNa	Cl	Intrus.	MixNa	Cl
18	Fresh.	Na	HCO ₃	Fresh.	Na	HCO ₃
19	Fresh.	Na	Cl	Intrus.	Na	Cl
LA				Fresh.	Na	Cl
ADE				Intrus.	Ca	HCO ₃
P Sar				Fresh.	Na	Cl
SAR 80				Fresh.	Na	Cl

In the HFE diagram for 2003, two of the four main facies can be identified: seven wells of Na-Cl facies (seawater dominant) and three that correspond to the Na-HCO₃ facies (salinized water with direct exchange). With respect to the subfacies, four samples correspond to MixNa-Cl; two to Na-MixCl; and one to each of the subfacies, Na-MixHCO₃, Mix Na –HCO₃, and MixCa-Cl.

In the HFE diagram, for 2014–2016, two of the four main facies can be identified: seven wells of Na-Cl facies (seawater dominant) and five that correspond to the Na-HCO₃ facies (salinized water with direct exchange). With respect to the subfacies, three samples correspond to MixNa-Cl and one to each of the four subfacies, Na-MixCl, Na-MixHCO₃, Mix Na–MixSO₄, and MixCa-MixCl.

The number of wells with seawater intrusion was constant between 2003 and 2014–2016 (10 samples correspond to freshwater and 9 to the intrusion facies), but wells 5 and 19 changed from freshwater in 2003 to intrusion in 2014–2016, and wells 15 and 8 refreshed in 2014–2016. In the freshwater group for 2014–2016, an average seawater fraction of 0.28 was obtained, as compared with 2.16 in the intrusion group. The four geothermal-influenced samples are included in the HFE diagram, but their position is not well represented. All three samples along the El Sargento fault are defined as freshwater, although their seawater fractions elevated from 3.1 to 88.5%. On the other hand, the least mineralized sample, ADE, which had a negative seawater fraction calculated, was classified in the HFE diagram as intrusion.

5. Geothermal Water

The results of field measurements (in situ) are reported in Table 7. The low redox values (maximum 20 mV, minimum –410 mV) exclude the presence of oxygen in the water, and, therefore, the measured oxygen concentrations are not reported. The concentrations of major cations and anions for all water samples included in Figure 11 are contained in Tables 8 and 9, respectively. The Charge–Balance Error (CBE) results were within an acceptable range ($\leq \pm 7\%$) for all water samples.

Table 7. The results of the physicochemical parameters, measured in the field.

Site	Key	pH	Temperature (°C)	Redox (mV)	Electrical Conductivity (µS/cm)
Los Angeles	LA	7.37	48.7	−157.5	5500
Agua Ademadas	ADE	6.59	26.8	−1163.1	120
La Ventana	VEN	7.09	32.3	−	2480
El Bajio	BAJ	7.69	38.6	−1139.8	960
Pozo Sargento	P Sar	7.91	29.0	−	5990
Sargento 80 °C	SAR 80	7.8	80.0	−	−
La Junta Creek *	BAR 1	9.49	25.6	−370.0	393
La Junta Creek *	BAR 3	9.33	26.4	−287.7	325
La Junta Creek *	BAR 5	9.61	26.1	−270.0	632
La Junta Creek *	BAR 11	9.44	28.5	−410.0	390
Buenavista **	BV	8.04	41.3	36.1	773
C. San Lucas 1 ***	SL1	6.9	25	−	1700
C. San Lucas 2 ***	SL2	6.4	22	−	3530
C. San Lucas 4 ***	SL4	5.6	42	−	28,200
C. San Lucas 5 ***	SL5	5.7	72	−	49,600
San Jose del Cabo. 6 ***	SJ6	7.3	36	−	6750
Seawater M7 ****	M7	7.8	25	−	−

* Wurl et al., 2014 [39]; ** Hernandez Morales and Wurl 2016 [57]; *** Lopez Sanchez et al. 2006 [56]; **** Prol-Ledesma et al., 2004 [17].

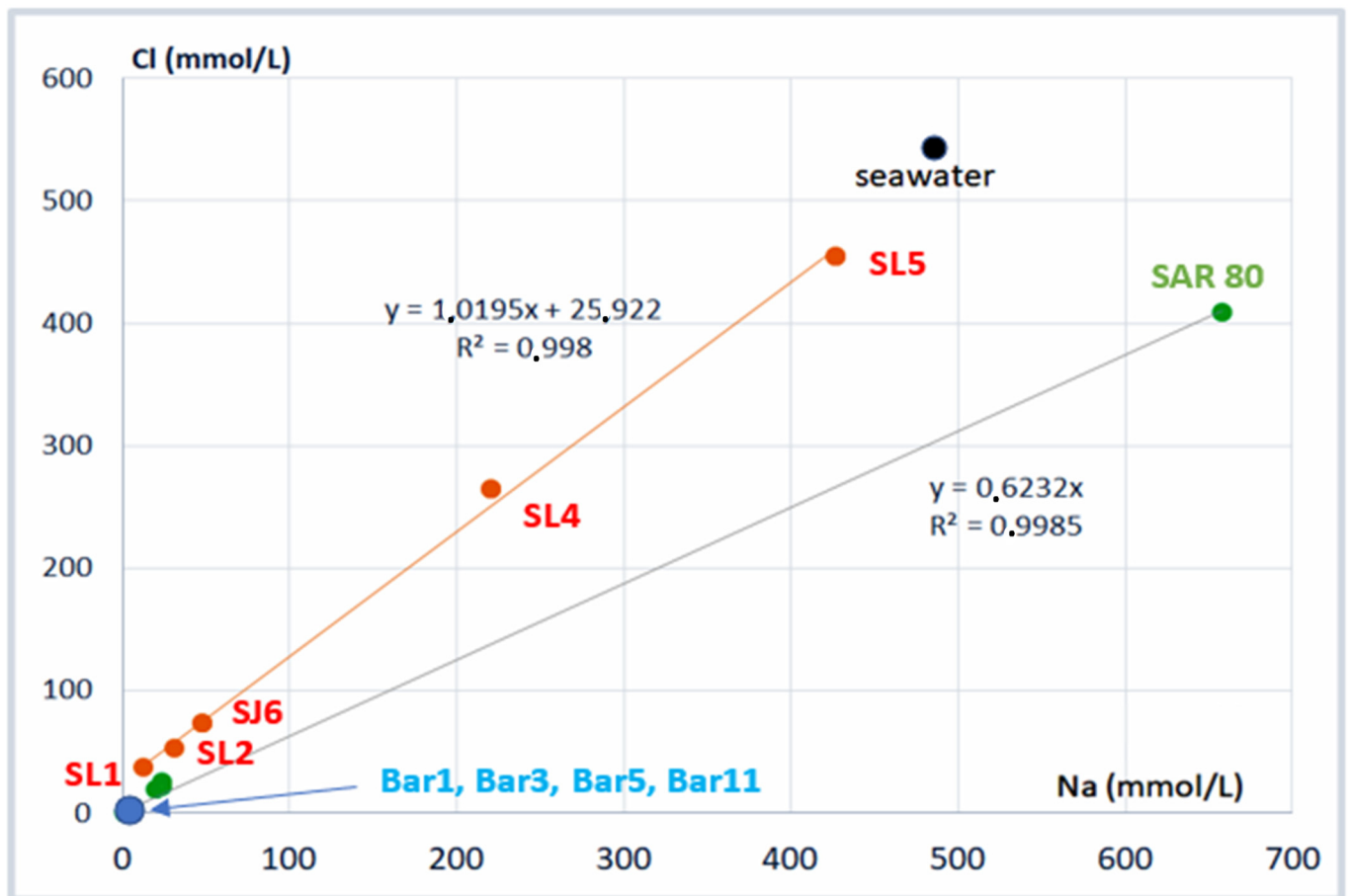


Figure 11. Scatter diagram of the relationship between Na and Cl in samples in Tables 7–9, visualizing the mixing between seawater and geothermal water.

Table 8. Concentration of main cations (mg/L).

Sample	Na	K	Ca	Mg	B
LA	460.6	15.0	68.6	8.9	1.1
ADE	29.9	0.5	40.0	6.2	0.1
VEN	550.0	19.6	105.6	67.6	–
BAJ	146.0	4.7	36.7	15.1	–
P Sar	554.5	9.2	60.8	30.7	1.0
SAR 80	15,136.9	509.0	589.1	569.4	8.2
Bar 1 *	90.2	1.5	2.0	0.1	9.5
Bar 3 *	97.5	1.2	2.6	0.1	6.0
Bar 5 *	87.9	1.4	1.9	0.1	0.8
Bar 11 *	85.2	0.5	4.8	0.2	2.0
BV **	152	4.31	5.2	0.63	0.3
SL1 ***	290.0	14.1	27.0	47.1	–
SL2 ***	722.0	35.0	32.0	59.0	–
SL4 ***	5070.0	283.0	1210.0	75.0	–
SL5 ***	9820.0	631.0	2430.0	69.6	–
SJ6 ***	1090.0	33.0	190.0	83.7	–
M7 ****	11,176.0	487.0	392.0	1400.0	–

* Wurl et al., 2014 [39]; ** Hernandez Morales and Wurl 2016 [57]; *** Lopez Sanchez et al. 2006 [56]; **** Prol-Ledesma et al., 2004 [17].

Table 9. Concentration of main anions (mg/L).

Sample	Cl	F	SO ₄	HCO ₃
LA	674.0	0.1	85.4	200
ADE	21.0	0.1	3.4	195
VEN	893.4	0.1	187.5	205.7
BAJ	158.1	0.1	55.0	170.0
P Sar	769.0	0.1	149.0	300
SAR 80	14,141.9	3.9	1670.6	100
Bar 1 *	58.3	1.8	56.3	70.3
Bar 3 *	88.6	3.2	33.6	75.8
Bar 5 *	53.0	0.6	48.6	237
Bar 11 *	36.5	2.3	40.8	59.7
BV **	121.5	2.22	59	7.2
SL1 ***	1279	0.1	105	371.9
SL2 ***	1826	0.1	200	278.9
SL4 ***	9132	1.7	625	93.0
SL5 ***	15,708	6.9	650	93.0
SJ6 ***	2557	2.9	500	325.4
M7 ****	18,744	0.1	2554	97.6

* Wurl et al., 2014 [39]; ** Hernandez Morales and Wurl 2016 [57]; *** Lopez Sanchez et al. 2006 [56]; **** Prol-Ledesma et al., 2004 [17].

Scatter diagrams were created to analyze the ratio of mixing between seawater and geothermal water samples from Los Planes. The relationship between Na and Cl was plotted for two types of thermal fluid: samples close to the El Sargento fault (green points in Figure 11) and samples described by Lopez-Sanchez et al. [56] (orange points in Figures 11 and 12). This comparison revealed a clear linear trend ($R^2 = 0.9985$) for the samples near the El Sargento fault, indicating a conservative mixing process between both fluids.

Two different main compositions of thermal water have been described for the Baja California Peninsula. The manifestations with the highest temperatures (SL5, SAR 80) were found near the coast [30,56,59], and in the case of SL5, seawater was identified as the main supply source, which is modified by geothermal processes [30,60,61]. This thermal water is enriched in Ca, As, Hg, Mn, Ba, HCO₃, Li, Sr, B, I, Cs, Fe, and Si relative to seawater [56,61]. The calculated temperatures for the deep reservoir reach 200 °C [56].

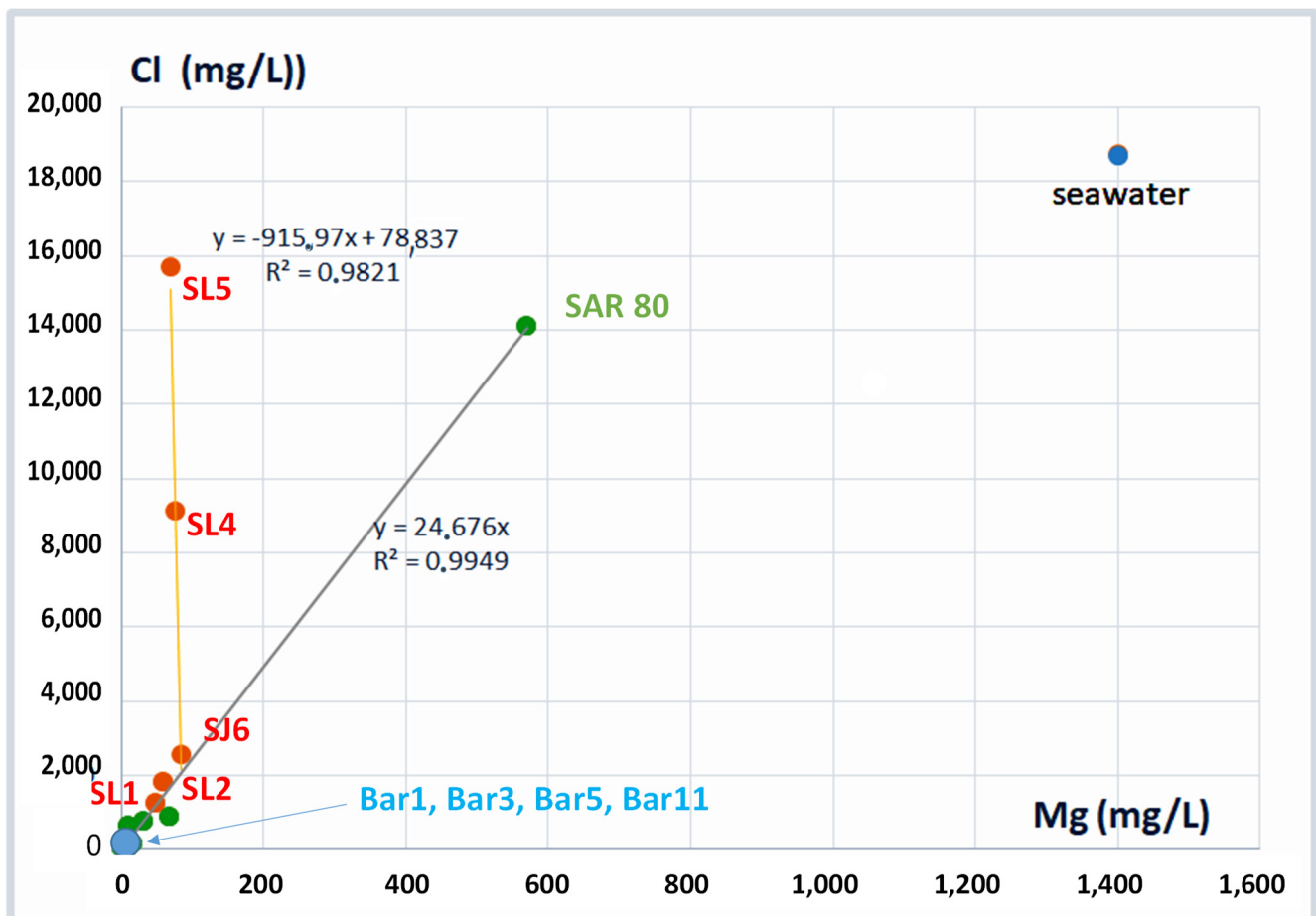


Figure 12. Scatter diagram of the relationship between Mg and Cl in samples in Tables 7–9, visualizing the mixing between seawater and geothermal water.

The relationship between Mg and Cl is presented in Figure 12. In this graph, three groups of water are identified. The first group corresponds to springs and wells in the La Junta area (Bars 1, 3, 5, and 11; blue dots) with the lowest Mg and Cl concentrations. The samples from Los Planes (green dots) and Cabo San Lucas (red dots) indicate a mixing process between seawater and thermal fluid. The thermal influence differs in both groups and can be recognized by the lower Mg content in the sample than in the seawater.

In contrast, Wurl et al. [39] and Hernández-Morales and Wurl [57], describe a different water composition for the thermal springs from the Los Cabos Block (Bar 1, Bar 3, Bar 5, and Bar 11), where meteoric water represents the main supply source. Here, very low mineralization and high pH values (up to 9.6) were observed. The calculated temperatures for the deep reservoir reach values between 86 °C and 115 °C (calculated with a quartz geothermometer) [62]. The highest temperature, measured at the surface, is less than 50 °C [57].

Mixtures between hydrothermal water and groundwater can be recognized based on elevated B/Cl ratios [63]. The following B/Cl ratios (for mg/L concentrations) were obtained: an average ratio of 0.075 for low mineralized thermal water, recharged by meteoric water (Bars 1,3, 5, and 11); higher mineralized thermal water with about 3% recharge from seawater 0.0016 (Los Angeles ranch); average seawater (0.00024); or freshwater (0.003 at LPL21). In the following section, the water samples are discussed based on scatter diagrams, as per the diagram proposed by Giggenbach and Goguel [55] (Figure 13).

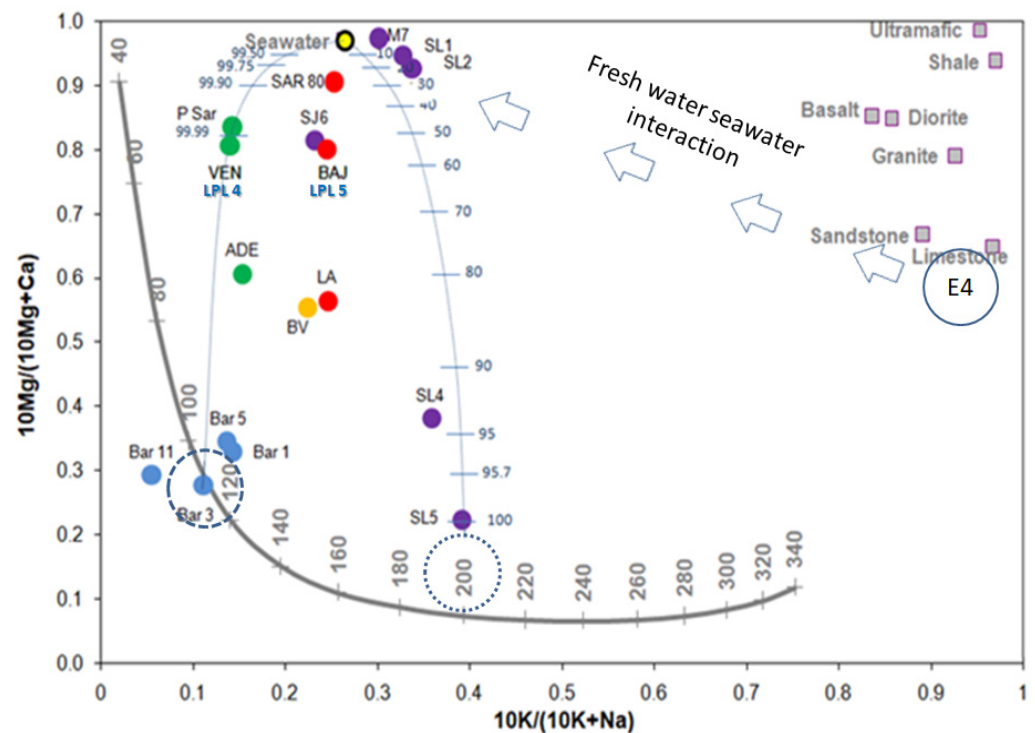


Figure 13. Diagram proposed by Giggenbach and Goguel [55] with all samples included and the percentage of mixing relationships between seawater and sample SL5 and Bar 3. Data were obtained from [11,30,39,56]. In the diagram taken from Giggenbach and Goguel [55], four water samples taken at thermal manifestations located near the La Junta creek in the Sierra la Laguna Mountains (Bar 1, Bar 3, Bar 5, and Bar 11 [39]) are closed to equilibrium conditions at a reservoir temperature between 100 and 110 °C. In the case of four wells drilled at the beach near Cabo San Lucas, only sample SL5 reaches the near-equilibrium temperature at 200 °C; the other three wells show mixtures with seawater in relationships of 7% at SL4, 70% at LS 2, and 80% at SL1. The seawater composition for the Gulf of California in Bahia Concepcion (M7), as described by Prol Ledesma [30], shows a slightly better fit with wells SL1 and SL2 than the composition of global seawater in Nordstrom et al. [64] (yellow circle in this figure).

Sample SL5 is representative of the thermal groundwater with seawater as the main source, and Bar 3 is typical for thermal water with meteoric water as the source, and these were recognized as endmembers. The resulting equilibrium temperatures of 200 °C and 110 °C for the deep reservoir coincide with the reported ones, obtained with different geo-thermometers by López-Sánchez et al. [56] and Wurl et al. [39]. Because the diagram permits the recognition of mixing processes between the different types of water [65], the mixing between both endmembers and seawater was calculated, and the mixing relation of different percentages was included in the diagram. The samples from the manifestation at Los Angeles and the thermal spring at the beach north of El Sargento coincide with those of Buenavista and San Jose del Cabo, indicating an intermediary position between both mixing lines, amounting to about 140–160 °C under equilibrium conditions and mixing with seawater. The shallow wells in the villages of El Sargento and La Ventana indicate lower equilibrium temperatures of 100–120 °C and mixing with less than 1% seawater. The fourth endmember (E 4 in Figure 13) is represented by the water–rock interaction with the sediment and was obtained from batch analyses conducted on sediments from the upper part of the aquifer (obtained from drillings in Briseño Arellano [15]; see Table 10). It represents the typical endmember for the pure reaction of rainwater with sediment.

Table 10. Typical endmember for the pure reaction of rainwater with sediment (obtained from batch analyses on sediments from the upper part of the aquifer), obtained from Briseño Arellano [15].

Sample	pH	Na	K	Ca	Mg	F	Cl	SO ₄	HCO ₃
07 PLRC 41	5.5	5.17	7.31	36.13	4.18	0.17	2.01	56.56	28.72
8 PLRC 103	5.5	3.96	6.32	40.45	5.28	0.23	1.67	99.3	27.28
10 PLRC 202	5.5	4.15	5.06	17.57	2.36	0.34	2.76	33.62	35.9
11 VWP3A	5.5	4.71	6.68	29.56	5.47	0	1.76	28.41	40.21
Mean value	5.5	4.27	6.02	29.19	4.37	0.19	2.06	53.78	34.46

6. Conclusions

Seawater intrusion contributes significantly to salinization, causing a decrease in groundwater quality and numerous environmental problems, such as high salinity levels, which may extend several kilometers inland in coastal aquifers. A negative effect on agriculture, water supply systems, and human health may result [41]. The existing methods cannot identify salinization due to mixing with mineralized thermal water. To recognize this additional impact, the differences in temperature and some dissolved solids allow us to distinguish between thermal water and typical surface water and groundwater. However, so far, only a few studies have focused on mixtures between thermal water and groundwater/surface water related to seawater intrusion.

Thus, the impact of higher mineralization caused by mixing with thermal water will not be recognized in most cases. In the case of the Los Planes aquifer, the elevated mineralization was reported correctly in former studies, but the influx of thermal water was confused with direct seawater introduced as an effect of ongoing aquifer overexploitation, which led to higher mineralization at the coastline; because of this, the water from most wells is not recommended for drinking. Our study indicates that the ongoing overextraction led to an average increase of 0.5% in the calculated seawater fraction since 2003. However, the Los Planes aquifer represents a complex system where thermal water affects groundwater quality in its western part. The geothermal manifestations along the faults of San Juan de Los Planes and El Sargento introduce thermal water with an important percentage of heated seawater into the aquifer. In a well near the Los Angeles ranch, we measured an increase in mineralization through thermal water, equivalent to 3.1 percent seawater. However, the water table indicates that this elevated mineralization cannot result from direct seawater inflow; rather, it is related to hydrothermal water with a mixture of seawater and freshwater as sources. This well is located on the El Sargento fault, where a gradual diminution of concentrations can be observed southward to the Sierra la Laguna Mountains, where meteoric water forms the source of the hydrothermal system. This low mineralized thermal water is associated with a rapid flow of meteoric water into deeper zones (reaching temperatures of around 100 °C) and a subsequent return to the surface [56]. The temperatures estimated for the deeper reservoir of the anomalies in the Los Planes aquifer at San Jose (SJ 6), El Bajio (BAJ), Los Angeles (LA), and El Sargento (SAR) show a tendency toward reservoir temperatures between 140 °C and 160 °C, providing several options for uses of this geothermal energy, for example, water desalination [66]. Future management strategies should be elaborated, taking into account our new findings.

Supplementary Materials: The datafile can be downloaded at: <https://www.mdpi.com/article/10.3390/resources12040047/s1>; Table S1: Groundwater; Table S2: Thermal water.

Author Contributions: Conceptualization, J.W. and M.A.I.-L.; methodology, J.W., M.A.I.-L. and L.C.M.-R. writing—original draft preparation, J.W., M.A.I.-L. and P.H.-M.; writing—review and editing, J.W., P.H.-M. and L.C.M.-R. visualization, M.A.I.-L., J.W. and P.H.-M. All authors have read and agreed to the published version of the manuscript.

Funding: This work was supported by the Mexican Secretariat of the Environment and Natural Resources [Grant No. SEMARNAT-2014-1-249423] within the project entitled “Effect of rainfall pattern on the concentration of trace elements in groundwater in arid areas”.

Informed Consent Statement: Not applicable.

Data Availability Statement: The following external datasets were used in this study: CNA, 2003: <http://defiendelasierra.org/wp-content/uploads/Estudio-CNA-Intrusion-Salina-y-Metales-Pesados-Los-Planes.pdf>; Briseño Arellano, 2014 (accessed on 16 January 2023): <http://132.248.9.195/ptd2014/agosto/0718072/0718072.pdf> (accessed on 16 January 2023).

Conflicts of Interest: The authors declare no conflict of interest.

References

1. Polemio, M.; Walraevens, K. Recent research results on groundwater resources and saltwater intrusion in a changing environment. *Water* **2019**, *11*, 1118. [[CrossRef](#)]
2. Ferguson, G.; Gleeson, T. Vulnerability of coastal aquifers to groundwater use and climate change. *Nat. Clim. Chang.* **2012**, *2*, 342–345. [[CrossRef](#)]
3. Werner, A.D.; Bakker, M.; Post, V.E.A.; Vandenbohede, A.; Lu, C.; Ataie-Ashtiani, B.; Simmons, C.T.; Barry, D.A. Seawater intrusion processes, investigation and management: Recent advances and futures challenges. *Adv. Water Resour.* **2013**, *51*, 3–26. [[CrossRef](#)]
4. Tran, D.A.; Tsujimura, M.; Pham, H.V.; Nguyen, T.V.; Ho, L.H.; Vo, P.L.; Ha, K.Q.; Dang, T.D.; Vinh, D.V.; Doan, Q.-V. Intensified salinity intrusion in coastal aquifers due to groundwater overextraction: A case study in the Mekong Delta, Vietnam. *Environ. Sci. Pollut. Res.* **2022**, *29*, 8996–9010. [[CrossRef](#)]
5. Mahlknecht, J.; Merchán, D.; Rosner, M.; Meixner, A.; Ledesma-Ruis, R. Assessing seawater intrusion in an arid coastal aquifer under high anthropogenic influence using major constituents, Sr and B isotopes in groundwater. *Sci. Total Environ.* **2017**, *587*, 282–295. [[CrossRef](#)]
6. Comisión Nacional de Agua. Estadísticas del Agua en México. 2018. Available online: http://sina.conagua.gob.mx/publicaciones/EAM_2018.pdf (accessed on 16 January 2023).
7. Sistema Nacional de Información del Agua (SNIA-CONAGUA). Tablas de Sobreexplotación y Salinización de Acuíferos en México para el Año 2021. 2021. Available online: <http://sina.conagua.gob.mx/sina/tema.php?tema=acuíferos> (accessed on 9 January 2023).
8. Fichera, M.M. Numerical Modeling and Hydrochemical Analysis of the Current and Future State of Seawater Intrusion in the Todos Santos Aquifer, Mexico. Ph.D. Thesis, Colorado State University, Fort Collins, CO, USA, 2019. Available online: https://mountainscholar.org/bitstream/handle/10217/195327/Fichera_colostate_0053N_15368.pdf (accessed on 16 January 2023).
9. Chávez-López, S.; Brito-Castillo, L. Calidad del agua subterránea en la Reserva de La Biosfera de El Vizcaino BCS, México. *Rev. Latinoam. Recur. Nat.* **2010**, *6*, 7–20.
10. González-Abraham, A.; Fagundo-Castillo, J.R.; Carrillo-Rivera, J.J.; Rodríguez-Estrella, R. Geoquímica de los sistemas de flujo de agua subterránea en rocas sedimentarias y vulcanogénicas de Loreto, BCS, México. *Bol. Soc. Geol. Mex.* **2012**, *6*, 319–333. [[CrossRef](#)]
11. Cardona, A.; Carrillo-Rivera, J.J.; Huizar-Alvarez, R.; Graniel-Castro, E. Salinization in coastal aquifers of arid zones: An example from Santo Domingo, Baja California Sur, Mexico. *Environ. Geol.* **2004**, *45*, 350–366. [[CrossRef](#)]
12. Wurl, J.; Gámez, A.E.; Ivanova-Boncheva, A.; Imaz-Lamadrid, M.A.; Hernández-Morales, P. Socio-hydrological resilience of an arid aquifer system, subject to changing climate and inadequate agricultural management: A case study from the Valle of Santo Domingo, México. *J. Hydrol.* **2018**, *559*, 486–498. [[CrossRef](#)]
13. Arango-Galván, C.; Prol-Ledesma, R.M.; Torres-Vera, M.A. Geothermal prospects in the Baja California Peninsula. *Geothermics* **2015**, *55*, 39–57. [[CrossRef](#)]
14. Comisión Nacional de Agua (CNA). Determinación de la Disponibilidad de Agua en el Acuífero (0323) Los Planes, Estado de Baja California Sur. 2003. Available online: <http://defiendelasierra.org/wp-content/uploads/Estudio-CNA-Intrusion-Salina-y-Metales-Pesados-Los-Planes.pdf> (accessed on 16 January 2023).
15. Briseño Arellano, 2014 Evaluación de la Evolución Hidrogeoquímica del Agua Subterránea en La Cuenca San Juan de Los Planes, Baja California Sur 2014 Tesis Lic. UNAM. Available online: <https://repositorio.unam.mx/covers/133713/0/300.png> (accessed on 16 January 2023).

16. Del Rosal Pardo, A. Recarga Natural en la Cuenca de San Juan de los Planes, Baja California Sur, México. Bachelor's Thesis, Universidad Autónoma de Baja California Sur, La Paz, México, 2003.
17. Busch, M.M.; Arrowsmith, J.R.; Umhoefer, P.J.; Cohan, J.A.; Maloney, S.J.; Gutiérrez, G.M. Geometry and evolution of rift-margin, normal-fault-bounded basins from gravity and geology, La Paz–Los Cabos region, Baja California Sur, Mexico. *Lithosphere* **2011**, *3*, 110–127. [[CrossRef](#)]
18. Cohan, M.M.; Arrowsmith, J.R.; Umhoefer, P.; Cohan, J.; Kent, G.; Driscoll, N.; Gutiérrez, G.M. Geometry and Quaternary slip behavior of the San Juan de los Planes and Saltillo fault zones, Baja California Sur, Mexico: Characterization of rift-margin normal faults. *Geosphere* **2013**, *9*, 426–443. [[CrossRef](#)]
19. NASA. NASA Shuttle Radar Topography Mission (SRTM) Version 3.0 (SRTM Plus) Product Release. Land Process Distributed Active Archive Center, National Aeronautics and Space Administration. 2013. Available online: <https://lpdaac.usgs.gov/news/nasa-shuttle-radar-topography-mission-srtm-version-30-srtm-plus-product-release/> (accessed on 28 October 2021).
20. Aranda-Gómez, J.J.; Pérez-Venzor, J.A. Estratigrafía del complejo cristalino de la región de Todos Santos, estado de Baja California Sur. *Revista* **1989**, *8*, 149–170.
21. Fletcher, J.M.; Kohn, B.P.; Foster, D.A.; Gleadow, A.J.W. Heterogeneous Neogene cooling and exhumation of the Los Cabos block, southern Baja California: Evidence from fission-track thermochronology. *Geology* **2000**, *28*, 107–110. [[CrossRef](#)]
22. Schaaf, P.; Böhnell, H.; Pérez-Venzor, J.A. Pre-Miocene palaeogeography of the Los Cabos block, Baja California Sur: Geochronological and palaeomagnetic constraints. *Tectonophysics* **2000**, *318*, 53–69. [[CrossRef](#)]
23. CONAGUA Comisión Nacional de Agua. Determinación de la Disponibilidad de Agua en el Acuífero (0323) Los Planes, Estado de Baja California Sur. 2020. Available online: https://sigagis.conagua.gob.mx/gas1/Edos_Acuiferos_18/BajaCaliforniaSur/DR_0323.pdf (accessed on 16 January 2023).
24. Wurl, J.; Martínez Gutiérrez, G. El efecto de ciclones tropicales sobre el clima en la cuenca de Santiago, Baja California Sur, México. In Proceedings of the III Simposio Internacional en Ingeniería y Ciencias para la Sustentabilidad Ambiental y Semana del Ambiente, Mexico City, Mexico, 5–6 June 2006.
25. Dominguez, C.; Magaña, V. The Role of Tropical Cyclones in Precipitation over the Tropical and Subtropical North America. *Front. Earth Sci.* **2018**, *6*, 19. [[CrossRef](#)]
26. Gutiérrez Caminero, L. Isótopos de Pb como Trazadores de Fuentes de Metales y Metaloides en el Distrito Minero San Antonio-El Triunfo, Baja California Sur. Master's Thesis, Centro de Investigación Científica y de Educación Superior de Ensenada, Ensenada, Mexico, 2013.
27. Aranda-Gómez, J.J.; Pérez-Venzor, J.A. *Excursión Geológica al Complejo Migmatítico de la Sierra de La Gata, BCS III Reunión Internacional Sobre la Geología de la Península de Baja California*; Sociedad Geológica Peninsular en la Universidad Autónoma de Baja California Sur: La Paz, Mexico, 1995; pp. 17–27.
28. CNA (Comisión Nacional del Agua), Gerencia de Aguas Subterránea. 1997; Estudio Hidrogeológico y Simulación Hidrodinámica del Acuífero del Valle de San Juan de los Planes, B.C.S. Final report; Dirección Local en Baja California Sur, unpublished.
29. Técnicas Modernas de la Ingeniería (TMI), S.A. 1977; Informe final del Estudio Geohidrológico del valle de San Juan de los Planes, en el estado de Baja California Sur, para la Subdirección de Geohidrología y de Zonas Áridas SARH, unpublished.
30. Prol-Ledesma, R.M.; Canet, C.; Torres-Vera, M.A.; Forrest, M.J.; Armienta, M.A. Vent fluid chemistry in Bahía Concepción coastal submarine hydrothermal system. *J. Volcanol. Geotherm. Res.* **2004**, *137*, 311–328. [[CrossRef](#)]
31. Prol-Ledesma, R.M.; Dando, P.R.; De Ronde, C.E.J. Special issue on shallow-water hydrothermal venting. *Chem. Geol.* **2005**, *224*, 1–4. [[CrossRef](#)]
32. Carrillo, A. Environmental Geochemistry of the San Antonio-El Triunfo Mining Area, Southernmost Baja California Peninsula Mexico. Ph.D. Thesis, University of Wyoming, Laramie, WY, USA, 1996.
33. COREMI (Consejo de Recursos Minerales). *Monografía Geológico-Minera del Estado de Baja California Sur*; Secretaría de Comercio y Fomento Industrial: Ciudad Juárez, México, 1999.
34. Carrillo-Chavez, A.; Drever, J.I.; Martinez, M. Arsenic content and groundwater geochemistry of the San Antonio-El Triunfo, Carrizal and Los Planes aquifers in southernmost Baja California, Mexico. *Environ. Geol.* **2000**, *39*, 1295–1303. [[CrossRef](#)]
35. Naranjo-Pulido, A.; Romero-Schmidt, H.; Mendez-Rodriguez, L.; Acosta-Vargas, B.; Ortega-Rubio, A. Soil arsenic contamination in the Cape Region, BCS, Mexico. *J. Environ. Biol.* **2002**, *23*, 347–352. [[PubMed](#)]
36. Carrillo, A.; Drever, J.I. Environmental assessment of the potential for arsenic leaching into groundwater from mine wastes in Baja California Sur, Mexico. *Geofísica Int.* **1998**, *37*, 35–39. [[CrossRef](#)]
37. Volke-Sepúlveda, T.; Solórzano-Ochoa, G.; Rosas-Domínguez, A.; Izumikawa, I.; Encarnación-Aguilar, G.; Velasco-Trejo, J.A.; Flores Martínez, S. Informe Final, Remediación de Sitios Contaminados por Metales Provenientes de Jales Mineros en Los Distritos de El Triunfo-San Antonio y Santa Rosalía, Baja California Sur, Mexico, 2003; 37p. Available online: <http://defiendelasierra.org/wp-content/uploads/Estudio-de-Remediación-de-Sitios-Contaminados-por-Metales-Provenientes-de-Jales-Mineros-en-Los-Distritos-de-El-Triunfo-y-Santa-Rosalía-2003.pdf> (accessed on 16 January 2023).
38. DVWK-Regeln Zur Wasserwirtschaft, H. Entnahme und Untersuchungsumfang von Grundwasserproben. In *DK 556.32.001.5 Grundwasseruntersuchung, DK 543.3.053 Probenahme. DVWK-Regeln zur Wasserwirtschaft 128, 36*; Deutscher Verband für Wasserwirtschaft und Kulturbau e.V.: Hamburg/Berlin, Germany, 1992. (In German)
39. Wurl, J.; Mendez-Rodriguez, L.; Acosta-Vargas, B. Arsenic content in groundwater from the southern part of the San Antonio-El Triunfo mining district, Baja California Sur, Mexico. *J. Hydrol.* **2014**, *518*, 447–459. [[CrossRef](#)]

40. U.S. Environmental Protection Agency. *Method 6020A—Inductively Coupled Plasma Mass Spectrometry*; Revision 1; U.S. Environmental Protection Agency: Washington, DC, USA, 2007.
41. Appelo, C.A.J.; Postma, D. *Geochemistry, Groundwater and Pollution*; A.A. Balkema: Rotterdam, The Netherlands, 1995.
42. Giménez-Forcada, E. Dynamic of Seawater Interface using Hydrochemical Facies Evolution Diagram (HFE-D). *Groundwater* **2010**, *48*, 212–216. [[CrossRef](#)]
43. Giménez-Forcada, E. Use of the Hydrochemical Facies Diagram (HFE-D) for the evaluation of salinization by seawater intrusion in the coastal Oropesa Plain: Comparative analysis with the coastal Vinaroz Plain, Spain. *HydroResearch* **2019**, *2*, 76–84. [[CrossRef](#)]
44. Ibrahim Hussein, H.A.; Ricka, A.; Kuchovsky, T.; El Osta, M.M. Groundwater hydrochemistry and origin in the south-eastern part of Wadi El Natrun, Egypt. *Arab. J. Geosci.* **2017**, *10*, 170. [[CrossRef](#)]
45. Klassen, J.; Allen, D.M.; Kirste, D. *Chemical Indicators of Salt Water Intrusion for the Gulf Islands, British Columbia*; Department of Earth Sciences, Simon Fraser University: Burnaby, BC, Canada, 2014; 43p.
46. Carreira, P.M.; Marques, J.M.; Nunes, D. Source of groundwater salinity in coastline aquifers based on environmental isotopes (Portugal): Natural vs. human interference. A review and reinterpretation. *Appl. Geochem.* **2014**, *41*, 163–175. [[CrossRef](#)]
47. Kelly, F. *Seawater Intrusion Topic Paper*; Island Country Health Department: Coupeville, WA, USA, 2005.
48. Anderson, W.P., Jr. Aquifer salinization from storm overwash. *J. Coast. Res.* **2002**, *18*, 413–420.
49. White, W.M. *Geochemistry*; John Wiley & Sons: Hoboken, NJ, USA, 2020.
50. Park, C.H.; Aral, M.M. Saltwater intrusion hydrodynamics in a tidal aquifer. *J. Hydrol. Eng.* **2008**, *13*, 863–872. [[CrossRef](#)]
51. Gupta, S.K.; Gupta, I.C. *Drinking Water Quality Assessment and Management*; Scientific Publishers: Jodhpur, India, 2020.
52. Edet, A. Hydrogeology and groundwater evaluation of a shallow coastal aquifer, southern Akwalbom State (Nigeria). *Appl. Water Sci.* **2017**, *7*, 2397–2412. [[CrossRef](#)]
53. Van Le, T.T.; Lertsirivorakul, R.; Bui, T.V.; Schulmeister, M.K. An application of HFE-D for evaluating seawater intrusion in coastal aquifers of Southern Vietnam. *Groundwater* **2020**, *58*, 1012–1022. [[CrossRef](#)]
54. Sajil Kumar, P.J. Deciphering the groundwater–saline water interaction in a complex coastal aquifer in South India using statistical and hydrochemical mixing models. *Model. Earth Syst. Environ.* **2016**, *2*, 1–11. [[CrossRef](#)]
55. Giggenbach, W.F.; Goguel, R.L. *Collection and Analysis of Geothermal and Volcanic Water and Gas Discharges*; Report No. CD 2401; Department of Scientific and Industrial Research, Chemistry Division: Petone, New Zealand, 1989.
56. López-Sánchez, A.; Bâncora-Alsina, C.; Prol-Ledesma, R.M.; Hiriart, G. A new geothermal resource in Los Cabos, Baja California Sur, Mexico. In Proceedings of the 28th New Zealand Geothermal Workshop, Auckland, New Zealand, 15–17 November 2006.
57. Hernández-Morales, P.; Wurl, J. Hydrogeochemical characterization of the thermal springs in northeastern of Los Cabos Block, Baja California Sur, Mexico. *Environ. Sci. Pollut. Res.* **2016**, *24*, 13184–13202. [[CrossRef](#)]
58. Stigter, T.Y.; Carvalho Dill, A.M.M.; Ribeiro, L.; Reis, E. Impact of the shift from groundwater to surface water irrigation on aquifer dynamics and hydrochemistry in a semi-arid region in the south of Portugal. *Agric. Water Manag.* **2006**, *85*, 121–132. [[CrossRef](#)]
59. Portugal, E.; Birkle, P.; Barragán, R.M.; Arellano, V.M.; Tello, E.; Tello, M. Hydrochemical-isotopic and hydrogeological conceptual model of the Las Tres Vírgenes geothermal field, Baja California Sur, México. *J. Volcanol. Geotherm. Res.* **2000**, *101*, 223–244. [[CrossRef](#)]
60. Canet, C.; Prol-Ledesma, R.M.; Proenza, J.A.; Rubio-Ramos, M.A.; Forrest, M.J.; Torres-Vera, M.A.; Rodríguez-Díaz, A.A. Mn–Ba–Hg mineralization at shallow submarine hydrothermal vents in Bahía Concepción, Baja California Sur, Mexico. *Chem. Geol.* **2005**, *224*, 96–112. [[CrossRef](#)]
61. Villanueva-Estrada, R.E.; Prol-Ledesma, R.M.; Torres-Alvarado, I.S.; Canet, C. Geochemical modeling of a Shallow Submarine Hydrothermal System at Bahía Concepción, Baja California Sur, México. In Proceedings of the World Geothermal Congress, Antalya, Turkey, 24–29 April 2005.
62. Verma, S.P.; Santoyo, E. New improved equations for Na/K, Na/Li and SiO₂ geothermometers by outlier detection and rejection. *J. Volcanol. Geotherm. Res.* **1997**, *79*, 9–24. [[CrossRef](#)]
63. Vengosh, A.; Gill, J.; Davisson, M.L.; Hudson, G.B. A multi-isotope (B, Sr, O, H, and C) and age dating (³H–³He and ¹⁴C) study of groundwater from Salinas Valley, California: Hydrochemistry, dynamics, and contamination processes. *Water Resour. Res.* **2002**, *38*, 9-1-9-17. [[CrossRef](#)]
64. Nordstrom, D.K.; Plummer, L.N.; Wigley, T.M.L.; Wolery, T.J.; Ball, J.W.; Jenne, E.A.; Bassett, R.L.; Crerar, D.A.; Florence, T.M.; Fritz, B. A Comparison of Computerized Chemical Models for Equilibrium Calculations in Aqueous Systems. In *Chemical Modeling in Aqueous Systems*; American Chemical Society: Washington, DC, USA, 1979; pp. 857–892. [[CrossRef](#)]
65. Powell, T.; Cumming, W. Spreadsheets for geothermal water and gas geochemistry. In Proceedings of the Thirty-Fifth Workshop on Geothermal Reservoir Engineering, Stanford, CA, USA, 1–3 February 2010. 10p.
66. Goosen, M.; Mahmoudi, H.; Ghaffour, N. Water desalination using geothermal energy. *Energies* **2010**, *3*, 1423–1442. [[CrossRef](#)]

Disclaimer/Publisher’s Note: The statements, opinions and data contained in all publications are solely those of the individual author(s) and contributor(s) and not of MDPI and/or the editor(s). MDPI and/or the editor(s) disclaim responsibility for any injury to people or property resulting from any ideas, methods, instructions or products referred to in the content.